ELSEVIER

Contents lists available at ScienceDirect

Chemical Engineering Journal

journal homepage: www.elsevier.com/locate/cej





Mechanistic insights into the efficient activation of peracetic acid by mackinawite (FeS) for diclofenac degradation under near-neutral conditions: Multiple identification and contribution of non-radicals

Yao-Feng Gao ^a, Yan-Ping Duan ^{a,b,*}, Yu-Ru Chen ^a, Yuan-Hua Jia ^a, Yao-Jen Tu ^{a,b}, Chao-Meng Dai ^{c,**}

- a Institute of Urban Studies, School of Environmental and Geographical Sciences, Shanghai Normal University, 100 Guilin Rd, Shanghai 200234, PR China
- b Yangtze River Delta Urban Wetland Ecosystem National Field Observation and Research Station, Shanghai 200234, PR China

ARTICLE INFO

Keywords: Peracetic acid FeS Diclofenac Single oxygen Mechanism

ABSTRACT

Peracetic acid (PAA) as an efficient, accessible, and environmentally friendly organic oxidizer will contribute to addressing the growing global issue of pharmaceutical contamination in aquatic environment. In this study, a low-cost and environmentally abundant mackinawite (FeS) was used to rapidly activate PAA to efficiently remove diclofenac (DCF). Over a wide pH range (3.0–8.0), the FeS/PAA system could achieve 80–100 % removal of DCF within 20 min. The $^{1}O_{2}$ -dominated non-radical played a dominant role in DCF degradation under nearneutral conditions. The possible degradation pathways of DCF were proposed, and the acute toxicity of DCF was significantly reduced after treatment by the FeS/PAA system. Cl^{-} , SO_{3}^{4} , NO_{3}^{-} , and HCO_{3}^{-} had virtually no substantive influence on the removal of DCF, while HA and CO_{3}^{2} had an inhibiting effect. In addition, the FeS/PAA system showed excellent anti-disturbance and decontamination abilities on multiple pharmaceuticals in real water samples, which demonstrated the potential application of the FeS/PAA system with a non-radical pathway in the treatment of pharmaceutical pollution in real water bodies. This study provides a new non-radical approach to degrade pharmaceuticals by efficiently activating PAA via heterogeneous FeS.

1. Introduction

Pharmaceutical environmental pollution has become a global issue [1,2]. Due to their low removal efficiency in traditional wastewater treatment plants, pharmaceuticals are frequently detected at level of ng/L to µg/L in various water bodies. Most pharmaceuticals exhibit low biodegradability, thus they can stay in the natural aquatic environment for a long time. Persistent pharmaceuticals in the aquatic environment can cause potential risks to aquatic organisms and ultimately threaten human health [3–6]. In particular, diclofenac (DCF), a non-steroidal anti-inflammatory pharmaceutical, has been considered the main reason for the extinction of the Indian vulture [7], and subsequent studies have reported the biotoxicity of DCF to other species [8]. Therefore, given their limited biodegradability and potential risks, it is imperative to develop effective technologies to degrade pharmaceuticals

in aquatic environment.

Recently, the advanced oxidation processes (AOPs) based on peracetic acid (PAA) have received increasing attention in pharmaceutical degradation due to the advantages of high oxidation potential (1.06 to 1.96 V) and limited toxic by-products formation [9–12]. Due to the lower bond energy of the O-O bond (159 kJ/mol), PAA is more easily activated to produce a series of reactive species (RS) such as •OH, organic radicals (R-O•), 1 O₂, etc, compared to the H₂O₂ (213 kJ/mol) and peroxymonosulfate (377 kJ/mol). PAA can be activated by various methods, such as UV irradiation [13], heat [14], transition metals (Mn (II), Fe(II), Cu (II), and Co(II)) [15–17], and activated carbon [18]. Especially, Fe(II) is an excellent activator for PAA due to its easy availability in the environment and low toxicity [19]. However, the homogeneous Fe(II) activation of PAA is restricted by acidic conditions, slow Fe(III)/Fe(II) circulation, and generation of iron sludge [19,20]. In

E-mail addresses: duanyanping@shnu.edu.cn (Y.-P. Duan), daichaomeng@tongji.edu.cn (C.-M. Dai).

^c College of Civil Engineering, Tongji University, 1239 Siping Road, Shanghai 200092, PR China

^{*} Corresponding author at: Institute of Urban Studies, School of Environmental and Geographical Sciences, Shanghai Normal University, 100 Guilin Rd., Shanghai 200234, PR China.

^{**} Corresponding author.

contrast, effective and stable heterogeneous Fe(II) (i.e. iron-based minerals) are highly desirable to advance the practical implementation of PAA. Recently, the application potential of sulfide ferrite has been mentioned. For example, Cheng et al. [21] discovered that S(-II) and sulfides could have an essential function in the Fe(III)/Fe(II) redox cycle, which can improve the utilization of Fe. Mackinawite (FeS) as one of the most abundant metal sulfide minerals in nature is commonly used as H₂O₂ and persulfate activator due to its ability to act as both a source of Fe(II) and as an electron donor [22,23]. FeS is low cost and has excellent catalytic performance, unlike other catalysts that need to carry out complex experimental modification [24-26], which is more conducive to the actual environmental applications. As a large abundance of natural minerals, FeS is environmentally friendly, and will not cause secondary pollution to the environment. Therefore, FeS-activated PAA has a great prospect for environmental application. Compared to experimentally synthesized FeS which generates toxic gases and high cost of chemical reagents during the synthesis process, commercial FeS is a mature product with stable specifications and guaranteed purity, and is more environmentally friendly and easy to scale up in the practical application. However, the research on PAA activation by FeS is very limited. Only one literature reported FeS used in the PAA activation system, but it focused on experimentally synthesized FeS rather than commercial FeS [27], in which they verified the facilitating role of S (-II) in the Fe(III)/Fe(II) cycle, and found that S species may consume R-O°, and •OH is the key RS for pharmaceuticals in the synthetic FeS/PAA system. While there is still a significant gap in understanding the activation mechanisms and S species's role of FeS in the PAA activating system. In particular, experimentally synthesized FeS and commercial FeS have different physical phase configurations, which are likely to affect the specific activation mechanism. Therefore, it is of great significance to further investigate the catalytic mechanisms, pharmaceutical degradation performance, and the influence factors of commercial FeS-activated PAA system in terms of practical application.

Previously, the reports based on activated PAA claimed that *OH, $R-O^{\bullet}$, and ${}^{1}O_{2}$, could potentially participate in pollutant removal as the main RS [24,28]. ¹O₂ is the high-energy state of the strongly reactive molecular oxygen [29]. Owing to its electrophilic nature, ¹O₂ is highly selective for electron-rich organic compounds [30]. ¹O₂, as a non-radical RS, is extremely compatible with water matrices, providing an unparalleled advantage over free radicals in practical applications [31]. However, some recent studies have questioned the identification, validity, and quantification of ¹O₂ [32–34]. Zong et al. [33] suggested that false-positive signals may occur in the conventional EPR test for ¹O₂ identification. Wang et al. [34] utilized a probe kinetic model to negate the validity of ¹O₂ for degradation of target pollutants as determined by scavenging experiments in Co₃O₄@CNTs activated persulfate systems. Zhu et al. [35] quantified the contribution of RS and non-radical pathways in sulfamethoxazole (SMX) removal in the MO₂C/PAA system based on a probe method, but the quantification was imperfect such as the absence of approximate exposure and transient concentrations of RS. Given the above controversies, it is therefore highly imperative to conduct an indepth study on the identification, validity, and quantification of RS in the activated PAA system.

In this study, we used commercial FeS to activate PAA for degrading pharmaceuticals. Diclofenac (DCF), which widely exists in natural water and has negative ecological effects, was selected as the target compound. The reaction mechanism was explored, including free radical and non-free radical pathways. The RS contributing to the degradation of DCF in the FeS/PAA process were systematically identified and quantified, and the validities were verified. The effects of the water matrix (pH, anion, and humic acid (HA)) on the stability of the natural FeS/PAA system were investigated in detail. Also, the degradation pathway of DCF in the natural FeS/PAA process was proposed based on DCF intermediates, and the toxicity variation of DCF was also evaluated by phytotoxicity tests. Finally, the applicability of the natural FeS/PAA system was evaluated in real water and multi-pharmaceutical systems.

To the best of our knowledge, this study is the first to reveal the non-radical pathway ($^{1}O_{2}$) in the natural FeS/PAA system, which provides new insights into the remediation of pharmaceutical pollution.

2. Materials and methods

2.1. Materials

(15 % w/w) PAA solution (20 % w/w H_2O_2) was purchased from Aladdin Co., Ltd. (Shanghai, China). Commercial FeS (chemically pure, purity is well over 70 %, the rest being iron and sulfur with no other disturbing impurities) was bought from Hushi-Sinopharm Chemical Reagent Co., Ltd. (Shanghai, China) and was ground and sieved through a filter of 100 mesh before use. Seeds were purchased from Lvbao Seed Industry (Shanxi, China) Co., Ltd. Other chemicals were listed in the Supporting Information Text S1 ("S" designates text, tables, and figures in the Supplemental Information here and thereafter). The real water samples were collected in February 2023 from the Taipu River monitoring station. The water samples were stored at 4 °C after being filtered through 0.45 μ m filters. The characteristic features of the water samples are shown in Table S1. The water used for all experiments was ultrapure (18.2 M Ω -cm), except for the real water test.

2.2. Experimental procedures

The degradation experiments were carried out in 100 mL of reaction solution in a 250 mL beaker at a temperature of $25\pm1^{\circ}C$ and a speed of 200 rpm with magnetic stirring. The initial pH was adjusted after the addition of a predetermined concentration of pharmaceuticals (DCF or probe compounds) using 0.1 M NaOH and H_2SO_4 . Subsequently, a predefined dose of FeS was added and mixed for 1 min to form a FeS-DCF suspension, and finally, the reaction was started by adding a predetermined dose of oxidant (PAA, H_2O_2). To avoid possible reactions between the RS and the buffer solution, no buffer solution was used in the experiments. After starting the reaction, 1 mL of the samples were picked up at specified intervals within 90 min, and the reaction was scavenged with 1 mL of $Na_2S_2O_3$ (4 g/L). The samples were filtered through a 0.22 μm filter membrane for further analysis. All experiments were repeated three times.

Quenching experiments were conducted by adding various scavengers (*tert*-butyl alcohol (TBA); furfuryl alcohol (FFA); 2,4-hexadiene (2,4-HD); p-Benzoquinone(BQ); L-histidine and methyl phenyl sulfoxide (PMSO)) into the system before the reaction. For the further evaluation of the $^1\mathrm{O}_2$ role in degrading DCF, a predetermined concentration of NaClO/H₂O₂ mixture was brought into the DCF solution to start the reaction. For the O $_2^{\bullet}$ degraded DCF evaluation experiments, DCF was added to the pyrogallol oxidation system (adding a predetermined concentration of pyrogallol in Tris-HCl buffer at pH 8 and waiting for pyrogallol autoxidation for 30 min) to initiate the reaction. The contribution of Fe(IV) to DCF removal was evaluated by employing the Fe(VI)/PAA system to initiate the reaction with the addition of PAA to the Fe(VI) solution contained DCF.

2.3. Probe-based kinetic model of the FeS/PAA system

Considering PAA direct oxidation, RS oxidation, and adsorption of FeS, the reduction of probe compounds in the FeS/PAA system follows Eq. (1). metronidazole (MDE) and methyl phenyl sulfoxide (PMSO) were chosen as the probe compounds for ${}^{1}O_{2}$ and Fe(IV), respectively, and the reduction of MDE and PMSO can be described by Eqs. (2) – (3).

Where [P] and [P₀] are the pollutant concentrations at time t and 0, respectively; k_{PAA} , $k_{^{1}\text{O}_{2}}$, and $k_{\text{Fe(IV)}}$ are pseudo-second-order rate constants (M $^{-1}$ s $^{-1}$) for the reaction of the pollutant with PAA, $^{1}\text{O}_{2}$, and Fe (IV); The k_{ads} is the pseudo-first order adsorption rate constant for the pollutant with FeS. \int [PAA]dt (M s) is the exposure amount of PAA,

Table 1Parameters for HPLC determination of compounds.

Compounds	Eluents	Wavelengths(nm)
DCF	Methanol: 0.1 %acetic acid = 70:30	275
MDE	Acetonitrile: water $= 20:80$	318
Florfenicol	Methanol: water $= 60:40$	220
Sulfamethoxazole	Methanol: 0.1 %acetic acid = 35:65	265
Sulfamethazine	Methanol: 0.1 %acetic acid = 25:75	265
Sulfathiazole	Methanol: 0.1 %acetic acid = 25:75	284
Chloramphenicol	Methanol: water $= 60:40$	278
PMSO	Acetonitrile: 0.1 %acetic acid = 70:30	230
PMSO ₂	Acetonitrile: 0.1 % acetic acid $= 70:30$	215

Table 2The pseudo-second rate constants for the reaction of the selected pollutants with PAA and RS.

Compounds	$k_{\mathrm{PAA}} (\mathrm{M}^{-1} \mathrm{s}^{-1})$	$k_{^{1}O_{2}}(M^{-1}s^{-1})$	$k_{\rm Fe(IV}) \ ({ m M}^{-1} { m s}^{-1})$
MDE PMSO DCF	0.00715 ^a 0.1425 ^a 0.06572 ^a	1.2×10^{8} [39] 2.61×10^{6} a 1.3×10^{7} [40]	$\begin{array}{c} 3.89 \times 10^{4} \ ^{a} \\ 1.23 \times 10^{5} \ \text{[41]} \\ 2.51 \times 10^{4} \ ^{a} \end{array}$

a measured in this study.

which can be determined from the integral of the decomposition curve of PAA. $\int [^1O_2]dt$ (M s) and $\int [Fe\ (IV)]dt$ (M s) are calculated from the binary equation Eqs. (2)–(3), which is based on reducing MDE and PMSO in the FeS/PAA system.

$$-ln\frac{[P]}{[P_0]} = k_{PAA} \int [PAA]dt + k_{^{1}O_2} \int \left[\ ^{1}O_2 \right] dt + k_{Fe(IV)} \int [Fe(IV)]dt + k_{ads}t \tag{1} \label{eq:local_part}$$

$$\begin{split} -ln\frac{[MDE]}{[MDE_0]} &= k_{PAA,MDE} \int [PAA]dt + k_{^1O_2,MDE} \int \left[\ ^1O_2 \right] dt \\ &\quad + k_{Fe(IV),MDE} \int \left[Fe(IV) \right] dt + k_{ads,MDE}t \end{split} \tag{2} \label{eq:2}$$

$$\begin{split} -ln \frac{[PMSO]}{[PMSO_0]} &= k_{PAA,PMSO} \int [PAA]dt + k_{^1O_2,PMSO} \int \left[\ ^1O_2 \right] dt \\ &+ k_{Fe(IV),PMSO} \int [Fe(IV)] dt + k_{ads,PMSO}t \end{split} \tag{3}$$

2.4. Analytical methods

The concentrations of pharmaceuticals, PMSO, and methyl phenyl sulfone (PMSO₂) were analyzed by high-performance liquid chromatography (HPLC, Agilent, USA) with a C18 column (5 μ m, 4.6 \times 250 mm) and a diode-array detector (DAD). Details of elution program of mobile phase and related parameters was also shown in Table 1. The concentrations of PAA and H2O2 in PAA solutions were measured by titration, and the concentration of PAA during the reaction was determined by spectrophotometric iodometry [36,37]. Electron paramagnetic resonance (EPR) studies were performed using a German Bruker A300. Characterization of FeS was carried out using a surface area and porosity analyzer (BET, Mac 2460), a scanning electron microscope (SEM, Gemini 300), X-ray diffraction (XRD, X'Pert PRO MPD), and X-ray photoelectron spectroscopy (XPS, Thermo Scientific K-Alpha), respectively. The degradation intermediates of DCF were analyzed by ultra-performance liquid chromatography-quadrupole-time-of-flight mass spectrometry (UPLC-Q-TOF-MS, Shimadzu Japan), and the parameters are described in detail in Text S2.

Direct methods were adopted to analyze the second-order rate constants of MDE and PMSO reactions with PAA [38]. Detailed experimental steps were given in Text S3 and Fig. S1. The second-order rate constants of pollutants with RS were obtained from the literature or measured by the complete kinetic method. Detailed experimental steps

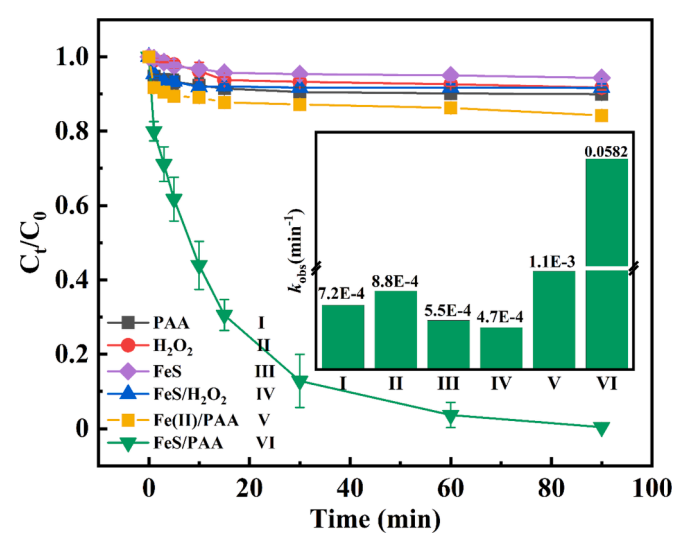


Fig.1. Removal of DCF in various systems. Conditions: [FeS] = 100 mg/L, [PAA] = $500 \mu M$, [DCF] = 1 mg/L, [H₂O₂] = 1.5 mM, [Fe(II)] = 1 mg/L, [pH] = 8, [pH] = 7.1 (H₂O₂,FeS/H₂O₂).

are described in Text S4. The pseudo-first-order adsorption rate constants of pollutants with FeS were analyzed from adsorption experiments. Detailed experimental steps are explained in Text S5, and results are given in Table S2. All the rate constants of compounds are listed in Table 2.

2.5. Toxicity test

Three types of beans (black, red, and mung) were used for phytotoxicity testing of DCF intermediates. Changes in the toxicity of the DCF intermediates were determined on account of growth (sprout rate and mean bud length). The ecotoxicity of DCF and its intermediates were also assessed using the ecological structure–activity relationship model (ECOSAR). The detailed procedure of the toxicity test is described in Text S6.

3. Results and discussion

3.1. Characterization of FeS

A series of characterizations were carried out to understand the nature of commercial FeS. The XRD pattern of FeS is shown in Fig. S4. The main diffraction peaks appeared at $2\theta = \text{of } 29.9^{\circ}$, 33.7° , 35.4° , 41.8° , 43.1° , 47.1° , 53.1° , 70.8° , 71.5° , respectively, with the FeS standard card (PDF#37–0477) (110), (112), (201), (203), (114), (221), (300), (224), and (118). These peaks are characteristic peaks of the FeS, indicating that the FeS mainly consisted of crystalline and cubic FeS. SEM results of FeS (Fig. S5) showed that the FeS particles before the reaction are irregular lumps, with a more uniform particle size, and the particle size ranges between 8 to 15 μ m. The FeS surface was stacked with many smaller-sized particles, which made the FeS surface show an uneven structure, and this structure might provide more reaction sites [42]. The EDS results (Fig. S5) showed that the Fe element was more distributed on the surface of FeS while the S element was dispersed on the surface of the Fe element, which might contribute to the rapid activation of PAA.

3.2. Assessment of the degradation effectiveness of DCF by the FeS/PAA system

To assess the DCF removal by FeS/PAA, Fe(II)/PAA, the PAA, H_2O_2 , and FeS alone systems were conducted. Fig. 1 showed the removal of DCF in various systems at pH = 8 (The pH of the H_2O_2 and FeS/ H_2O_2

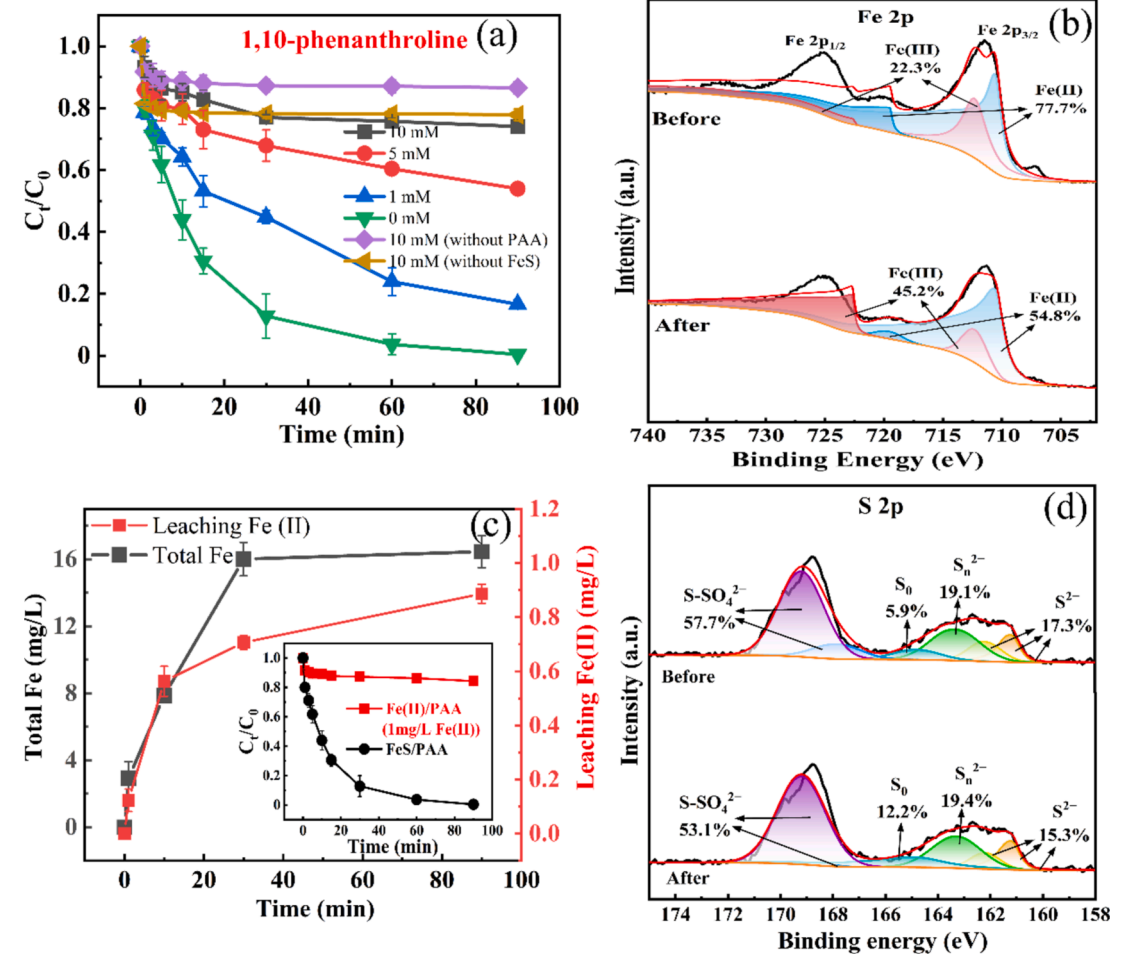


Fig.2. (a) Influence of 1,10-Phenanthroline on DCF removal; (b) XPS spectrum of the Fe 2p region of FeS before and after reaction; (c) Total and leaching Fe(II) concentrations in FeS/PAA system and DCF removal in leaching Fe(II)/PAA system; (d) XPS spectrum of the S 2p region of FeS before and after reaction. Conditions: $[FeS] = 100 \text{ mg/L}, [PAA] = 500 \mu\text{M}, [DCF] = 1 \text{ mg/L}, [pH] = 8.$

system was 7.1, considering that the addition of 500 μM PAA causes the pH in the system to decrease from 8 to 7.1, whereas H₂O₂ does not cause a pH change.). It can be seen that the negligible removal of DCF by FeS, PAA, and H₂O₂ alone, suggests that FeS, PAA, or H₂O₂ alone could not adsorb or directly oxidize DCF under near-neutral condition. As the PAA solution coexisted with H₂O₂, the effect of H₂O₂ in removing DCF was considered. In the FeS/H₂O₂ system, only 8.3 % of DCF was removed, indicating little role of $\mathrm{H_2O_2}$ for DCF removal. The DFC removal by the FeS/PAA system achieved about 80 % within 20 min, and nearly 50 % of DFC was removed within 5 min ($k_{\rm obs} = 0.0582~{\rm min}^{-1}$), which followed pseudo-first-order kinetics. $k_{\rm obs}$ showed a linear relationship with both the dosage of FeS ($R^2 = 0.9250$) and PAA ($R^2 = 0.9717$) when the dosage of FeS was increased from 25 mg/L to 150 mg/L (Fig. S6) and PAA was increased from $100 \, \mu M$ to $600 \, \mu M$ (Fig. S7). Considering the dosage cost and utility, FeS = 100 mg/L and PAA = 500 μM have satisfied the DCF for efficient removal, so they were selected as the optimal dosage. This result demonstrated that the FeS/PAA system could be effectively applied to remove DCF. Comparatively, the removal of DCF in the Fe (II)/PAA systems was only 16.7 % at pH = 8, which could explain that the effectiveness of the homogeneous activation system is highly dependent on the acidic conditions [19,43-45]. Therefore, it could be deduced that the DCF removal was attributed to the excellent activation of PAA by FeS.

To further verify the activation of PAA by FeS, the changes in the concentration of PAA were monitored in the FeS/PAA system. As depicted in Fig. S8, PAA was quickly decomposed under the activation of

FeS, and the tendency of PAA decomposition and DCF degradation remained consistent. Furthermore, the variation of FeS in particle morphology and surface elements before and after the reaction (Fig. S5) also proved that FeS had participated in the activation process of PAA. These results indicated that FeS would activate PAA effectively.

3.3. Mechanism of PAA activation by FeS

3.3.1. Identification of activation triggers

It is well established that the catalyst for activating PAA is Fe(II) rather than S [20,27,45]. To take insurance, we utilized the Na₂S-activated PAA system to remove DCF to determine the possible activation of PAA by $S(-II)/S^{2-}$. As a result, the removal of DCF by the Na₂S/PAA system and the PAA alone system was almost the same (Fig. S9), which excluded the activation effect of S to PAA. To confirm that Fe(II) activates PAA, 1,10-phenanthroline was used as a chelator for Fe(II). 1,10phenanthroline is typically a strong chelator that forms stable complexes with Fe(II), thereby preventing the electron transfer of Fe(II). As expected, the removal of DCF was inhibited in the presence of 1,10-phenanthroline, and the removal of DCF decreased from 99.6 % to 25.9 % at a concentration of 10 mM 1,10-phenanthroline (Fig. 2a). To investigate the activated mechanism of FeS to PAA, XPS spectrum analysis of FeS before and after the reaction was used to reveal the changes in the surface elemental composition and valence state on the FeS surface. As shown in Fig. 2b, the characteristic peaks with binding energies of 710.6 eV and 719.5 eV on the Fe2p orbital represent Fe(II), and the

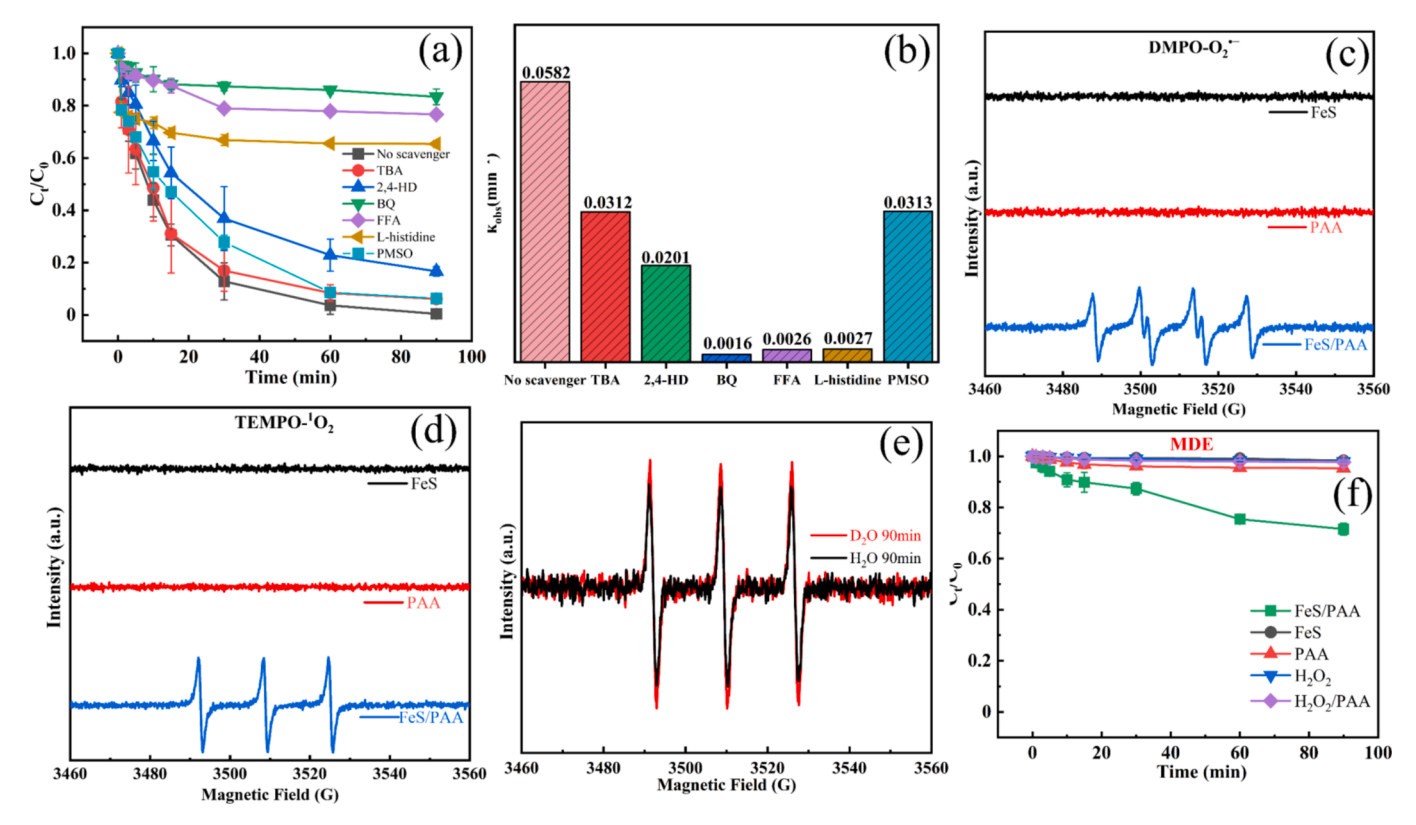


Fig. 3. (a) Quenching effect of various scavengers on the removal of DCF in the FeS/PAA system; (b) The variation $k_{\rm obs}$ of various scavengers; The EPR spectra using (c) DMPO and (d, e) TEMPO as spin-trapping agent in the FeS/PAA system; (f) Degradation of MDE in various reaction systems. Conditions: [TBA] = 200 mM, [2,4-HD] = 30 mM, [BQ] = 50 mM, [FFA] = 200 mM, [L-Histidine] = 200 mM, [PMSO] = 10 mM, [FeS] = 100 mg/L, [PAA] = 500 μM, [DCF] = 1 mg/L, [MDE] = 1 mg/L, [DMPO] = 100 mM, [TEMPO] = 100 mM, [PH] = 8.

characteristic peaks with binding energies of 712.3 eV and 722.7 eV represent Fe(III). Before the reaction, the proportions of Fe(II) and Fe (III) were 77.7 % and 22.3 %, respectively, while after the reaction, the proportion of Fe(II) decreased to 54.8 % and the proportion of Fe(III) increased to 45.2 %, which indicated that Fe(II) on the surface of FeS was involved in and oxidized to Fe(III) during the reaction. This further proved that it was Fe(II) that dominated the activation of PAA. Notably, total Fe and leaching Fe(II) were also monitored during the reaction. As shown in Fig. 2c, very little Fe(II) was leached (less than 1 mg/L). Compared with the FeS/PAA system (99.6 %), limited removal of DCF (16.7 %) was observed in the Fe(II)/PAA system, in which the initial Fe (II) concentration was 1 mg/L (Fig. 2c). According to these results, we could deduce that the heterogeneous Fe(II) on the FeS surface acted as the dominated active site to activate PAA, and dissolved Fe(II) had a little contribution to DCF removal in the FeS/PAA system.

It was reported that S^{2-} had a facilitating function in the Fe(II)/Fe (III) cycle [21,27,46]. S^{2-} could act as an electron donor for the reduction of Fe(III) to yield Fe(II) (Eq. (4)) [47]. Fig. 2d depicts the XPS spectrum of S 2p. The characteristic peaks of S^{2-} , S-SO $_4^{2-}$, S_n^{2-} and S_0 were observed. The proportion of S-SO $_4^{2-}$ was higher than that of S^{2-} , probably due to the partial oxidation of S. After the reaction, the percentage of S^{2-} dropped from 17.3 % to 15.3 %, suggesting the oxidation of S^{2-} and the possible provision of electrons to promote Fe(II)/Fe(III) cycle (Eq. (4)).

$$S^{2-} + Fe(III) + 4H_2O \rightarrow Fe(II) + SO_4^{2-} + 8H^+$$
 (4)

3.3.2. Identification of RS in the near-neutral FeS/PAA system

In previous studies, Fe(II)-based PAA-activated systems can generate RS, such as \bullet OH, R - O $^{\bullet}$, and O $^{\bullet}$ $^{-}$ radicals, 1 O₂, as well as Fe(IV) (Eps. (5) - (18)), and these RS played important roles in the degradation of

organic pollutants [19,27,31,48-51].

$$H_2O_2 + Fe(II) \rightarrow H_2O + Fe^{IV}O^{2+}$$
 (5)

$$H_2O_2 + Fe(II) \rightarrow \bullet OH + Fe(III) + OH^-$$
 (6)

$$CH_3C(O) \bullet OH + Fe(II) \rightarrow CH_3C(O)OH + Fe^{IV}O^{2+}$$
 (7)

$$CH_3C(O)OOH + Fe(II) \rightarrow CH_3C(O)O \bullet + Fe(III) + OH^-$$
 (8)

$$CH_3C(O)OOH + Fe(II) \rightarrow CH_3C(O)O^- + Fe(III) + \bullet OH$$
(9)

$$CH_3C(O)OOH + Fe(III) \rightarrow CH_3C(O)OO \bullet + Fe(II) + H^+$$
 (10)

$$CH_3C(O)OOH + CH_3C(O)O \bullet \rightarrow CH_3C(O)OO \bullet + CH_3C(O)OH$$
 (11)

$$CH_3C(O)OOH + \bullet OH \rightarrow CH_3C(O)OO \bullet + H_2O$$
(12)

$$CH_3C(O)OOH + CH_3C(O)OO^- \rightarrow CH_3C(O)OH + CH_3C(O)O^- + {}^1O_2$$
 (13)

$$Fe(II) + O_2 \rightarrow Fe(III) + O_2^{\bullet -}$$
(14)

$$H_2O_2 + \bullet OH \rightarrow H_2O + O_2^{\bullet -} \tag{15}$$

$$\bullet OH + O_2^{\bullet -} \rightarrow OH^- + {}^1O_2 \tag{16}$$

$$2O_2^{\bullet -} + 2H_2O \rightarrow H_2O_2 + 2OH^- + {}^1O_2$$
 (17)

$$O_2^{\bullet -} + H_2 O_2 \rightarrow \bullet OH + OH^- + {}^1O_2$$
 (18)

To identify the contribution of these RS in DCF removal, quenching experiments were conducted. For determining the free radicals in the FeS/PAA system, high concentrations of TBA, 2,4-HD, and BQ were selected as scavengers. Figure S10a shows that the addition of TBA, 2,4-HD, and BQ had a minor effect on PAA consumption, suggesting that the inhibition of DCF degradation was not primarily caused by the consumption of PAA by the scavengers. TBA is a well-known •OH scavenger

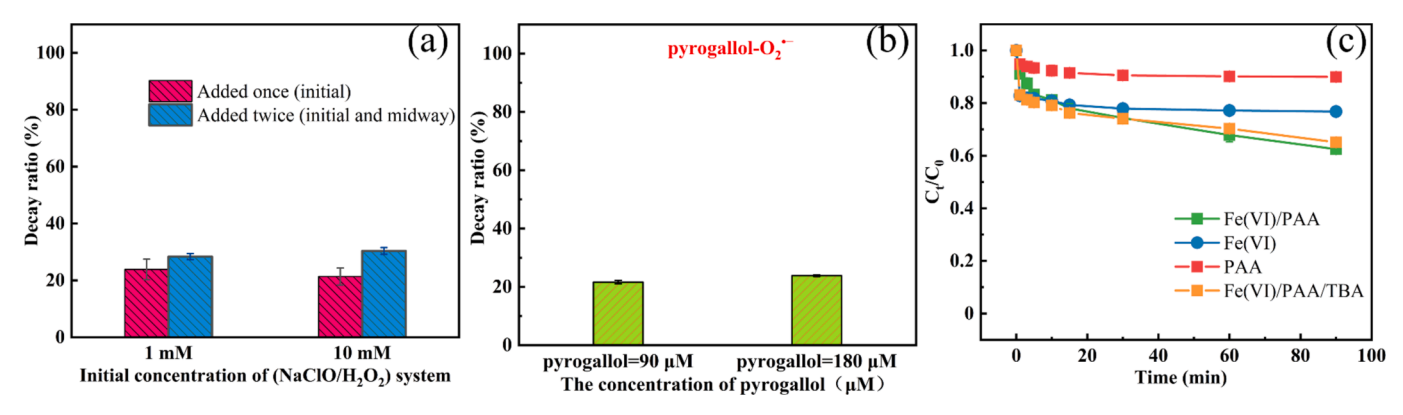


Fig. 4. Controlled experiments of ${}^{1}O_{2}$ (a), $O_{2}^{\bullet-}$ (b) and Fe(IV) (c) on the degradation of DCF. Conditions: [PAA] = 500 μ M, [DCF] = 1 mg/L, [Fe(VI)] = 500 μ M, [pH] = 9

 $(k_{\text{TBA},\bullet\text{OH}} = 6.0 \times 10^8 \,\text{M}^{-1} \,\text{S}^{-1}). \, 2,4\text{-HD could scavenge both R} - \text{O}^{\bullet} \, (k_2, \text{CO})$ $_{\text{4-HD. R-O}}$ = 9.2 × 10⁸ M⁻¹ S⁻¹) and $_{\text{OH}}$ ($k_{2,4\text{-HD}}$, $_{\text{OH}}$ = 9.16 × 10⁹ M⁻¹ S⁻¹) [52,53]. The excess TBA and 2,4-HD were added to the FeS/PAA system to evaluate the contribution of $\bullet OH$ and $R-O^{\bullet}$. As shown in Fig. 3a, b and Fig. S11a, TBA (($k_{\rm obs}=0.0312~{\rm min}^{-1}$) had almost no inhibition on the DCF removal in the FeS/PAA system, indicating that •OH was not the dominating RS in DCF removal in the FeS/PAA system, which is different from the results based on the synthetic FeS/PAA system in a previous study [27]. The inhibition of DCF removal by 2,4-HD ($k_{\rm obs} = 0.0201~{\rm min}^{-1}$) suggested that R – O $^{\bullet}$ may be the RS involved in DCF removal. However, we found that 2,4-HD inhibited the decomposition of PAA in the FeS/PAA system (Fig. S10b), suggesting that the inhibition of DCF removal by 2,4-HD was likely due to the inhibition of PAA decomposition. To further test the \bullet OH and R - O $^{\bullet}$ in the FeS/PAA system, EPR test using DMPO as the spin-trapping agent was conducted. As shown in Fig. S12, although the signal of DMPO-●OH was observed in the FeS/PAA system, the intensities were very weak. No typical signal of DMPO-R-O was observed in the FeS/PAA system further confirmed that R-O was not the main RS caused by the removal of DCF. To determine the contribution of $O_2^{\bullet -}$ for the DCF removal in the FeS/PAA system, BQ ($k_{O_2^{\bullet -},BQ} = 1.2 \times 10^9 \text{M}^{-1} \text{ S}^{-1}$) [54] was introduced as a scavenger. The results showed that DCF removal was significantly inhibited and that PAA decomposition was not affected by BQ (Fig. 3a, Fig. S10b, and Fig. S11). The DCF removal decreased to 16.6 % in the presence of 50 mM BQ, and the significant inhibition emphasized the crucial role of O_2^{\bullet} in DCF removal. The corresponding EPR test (Fig. 3c) also showed a typical DMPO-O $_2^{\bullet}$ - signal in the FeS/PAA system. Based on these results, we inferred that O_2^{\bullet} could be an important RS engaged in DCF removal in the free radical oxidation pathway.

For insight into the reaction mechanism, the possible non-radicals ((Fe(IV) and ¹O₂)) in this study were investigated. Previous studies proved that Fe(IV) instead of Fe(V) may be yielded in Fe-based catalyst AOPs and can oxidize certain organics ($k = 8 \times 10^1 \, \text{M}^{-1} \, \text{S}^{-1}$ to 3×10^5 $\mathrm{M}^{-1}~\mathrm{S}^{-1}$) [55–57]. Since PMSO could selectively yield PMSO₂ with Fe (IV) by oxygen transfer (k $_{Fe(IV),~PMSO}=1.23\times10^5~M^{-1}~S^{-1})$ [41], the excess PMSO (10 mM) was used for the scavenging experiments and a low concentration of PMSO (1 mM) was used for the probe experiments. Fig. S10 demonstrated that the consumption effect of PMSO to PAA was minimal and hardly affected the decomposition of PAA in the FeS/PAA system. The results (Fig. 3a) revealed that DCF removal was slightly inhibited in the presence of PMSO, indicating that Fe (IV) might participate in the removal of DCF, but its contribution was minimal. In the probe experiments, PMSO gradually decayed and PMSO2 was continuously generated as the reaction proceeded, proving the existence of Fe(IV) (Fig.S13). Eventually, the molar ratio of the amount of PMSO₂ yielded to the amount of PMSO decayed was 41.6:275. The generation of PMSO₂ was much smaller than the reduction of PMSO, probably due to the oxidation of PMSO by PAA, as evidenced by the control experiments (Fig. S14). Based on the scavenging and probe experiments, we inferred that trace amounts of Fe(IV) were yielded in the FeS/PAA system, and it has a certain contribution to the degradation of DCF.

Since the identification of ${}^{1}O_{2}$ has become partially controversial in recent years [32-34], four methods were used to identify ¹O₂ in this study. FFA (k $_{^{1}O_{2}, \, FFA}=1.2\times 10^{8}~M^{-1}~S^{-1}$) [58] and L-histidine (k $_{^{1}O_{2}, \, L-histidine}=3.24\times 10^{7}~M^{-1}S^{-1}$) [40] were chosen as scavengers of ¹O₂. The results (Fig. 3a) that the presence of both FFA and L-histidine at high concentrations significantly suppressed the removal of DCF, and the suppression influence was positively associated with the concentration of the scavengers (Fig. S15). The removal of DCF dropped to 23.4 % and 34.6 %, respectively, in the presence of 200 mM FFA and 200 mM L-histidine. The results indicated that ¹O₂ may be a crucial RS involved in DCF removal. Although we found that FFA and L-histidine consumed PAA slightly more than the other scavengers and caused some inhibition of PAA decomposition in the FeS/PAA system (Fig. S10), this was not sufficient to cause a strong inhibition of DCF removal (FFA: $k_{obs} =$ $0.0026 \,\mathrm{min}^{-1}$, L-histidine: $k_{\mathrm{obs}} = 0.0027 \,\mathrm{min}^{-1}$), and it is the quenching of ¹O₂ that is more likely to be responsible for the strong inhibition of DCF removal. Furthermore, the prominent TEMPO-¹O₂ signals (1:1:1 intensity ratio triplet line) in the EPR test (Fig. 3d) further indicated the existence of ¹O₂ in the FeS/PAA system. Previous studies have illustrated that ${}^{1}O_{2}$ is more active in $D_{2}O$ and has a stronger TEMPO- ${}^{1}O_{2}$ spectral signal due to the much shorter lifetime of ${}^{1}O_{2}$ in $H_{2}O$ (3.5 μ s) than that in D_2O (67 µs) [32,59–61]. We compared the removal of DCF in the FeS/ PAA-D₂O system and the FeS/PAA-H₂O system. It was found (Fig. S16) that the removal rate of DCF was indeed higher in the FeS/PAA-D2O system. The EPR test also showed a stronger triplet line signal in the FeS/ PAA-D₂O system (Fig. 3e), which further proved the presence of ¹O₂ in the FeS/PAA system. Furthermore, we adopted MDE as a probe compound for 1O_2 (k $_{^1O_2,\,MDE}=1.2\times 10^8~M^{-1}\ S^{-1})$ [39] to carry out the probe experiments. The results showed that MDE achieved 28.5 % removal in the FeS/PAA system (Fig. 3f). The control experiments of other systems, also revealed that the MDE removal was primarily due to $^{1}\mathrm{O}_{2}$ oxidation rather than FeS adsorption, direct oxidation by PAA and H₂O₂, and the FeS/H₂O₂ system. With the synergistic identification of the four approaches, we inferred that ¹O₂ may be the dominant RS for DCF removal in the FeS/PAA system.

3.3.3. The verification of DCF degradation by RS

Most of the previous studies focused only on the identification of the RS in the AOPs system, without addressing whether the identified RS were able to degrade the target pollutants[33,62]. This would result in incorrect identification of the RS, which may not react with the target pollutants [34,63,64]. Thus, the validity of three RS ($^1\mathrm{O}_2$, O_2^{\bullet} $^-$ and Fe (IV)) for DCF degradation was investigated to further confirm the validity of the identification of RS in the FeS/PAA.

¹O₂ can directly oxidize organics containing unsaturated bonds by

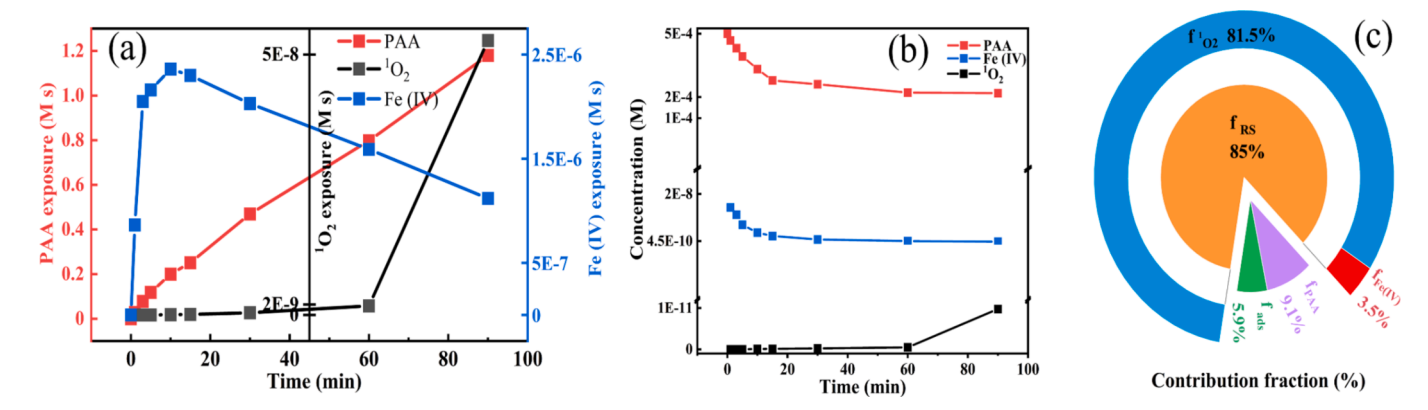


Fig.5. (a) Evolution of the exposure amount (a) and concentrations (b) of PAA, $^{1}O_{2}$, and Fe(IV) during DCF degradation in FeS/PAA systems; (c) Contribution of PAA oxidation (f $_{PAA}$), $^{1}O_{2}$ oxidation (f $_{PAA}$), $^{1}O_{2}$ oxidation (f $_{PAA}$), Fe(IV) oxidation (f $_{Fe(IV)}$), and the adsorption of FeS for DCF in the FeS/PAA system. Conditions: [DCF] = 1 mg/L, [FeS] = 100 mg/L, [PAA] = 500 μ M, [PMSO] = 10 μ M, [MDE] = 1 mg/L, [PH] = 8.

electron transfer or electrophilic addition and exhibited high reactivity with organics containing electron-rich groups [30,65–67]. As DCF is an organic compound containing electron-rich groups, previous studies have confirmed the high reactivity of $^{1}\mathrm{O}_{2}$ with DCF (k $_{^{1}\mathrm{O}_{2},\mathrm{DCF}}=1.3\times10^{7}\,\mathrm{M}^{-1}\,\mathrm{S}^{-1})$ [40], suggesting that $^{1}\mathrm{O}_{2}$ can be prone to degrade DFC. To clarify the efficiency of DCF degradation by $^{1}\mathrm{O}_{2}$, the $\mathrm{H}_{2}\mathrm{O}_{2}/\mathrm{NaClO}$ system was chosen as the benchmark system for the generation of $^{1}\mathrm{O}_{2}$. Because it has been convincingly validated to produce a high yield (80 - 100 %) of $^{1}\mathrm{O}_{2}$, and no production of intermediate radicals (Eq. (19)) [68,69]. As shown in Fig. 4a, obvious removal of DCF (23.9 % - 30.4 %) was achieved within 90 mi at 1 mM and 10 mM system concentrations, whether $\mathrm{H}_{2}\mathrm{O}_{2}/\mathrm{NaClO}$ was added only once or twice. This means that $^{1}\mathrm{O}_{2}$ can achieve the degradation of DCF. The high reactivity and excellent degradation performance of $^{1}\mathrm{O}_{2}$ for DCF confirmed that $^{1}\mathrm{O}_{2}$ can effectively remove DCF in the FeS/PAA system.

$$H_2O_2 + ClO^- \rightarrow {}^1O_2 + H_2O + Cl^-$$
 (19)
 $k = 3.4 \times 10^3 M^{-1} S^{-1}$.

 O_2^{\bullet} has a reduction potential of -0.33 V and a half-life of from s to min in water [70-72]. It is mainly involved in degrading pollutants through disproportionation, single electron transfer, deprotonation, and nucleophilic substitution [73]. Pyrogallol autoxidation was used as a benchmark system for O_2^{\bullet} generation [74]. DCF also demonstrated a favorable removal efficiency (~23 %) in the various concentrations of pyrogallol systems (Fig. 4b), implying that O_2^{\bullet} was feasible as a RS. However, in recent years, some studies pointed out that O_2^{\bullet} was particularly sensitive to converted to 1O_2 via disproportionation (Eq. (17)) and Haber-Weiss reaction (Eq. (18)) [75,76], which means that O_2^{\bullet} is primarily an intermediate for the generation of ${}^{1}O_{2}$ [77,78]. This is an important reason why the presence of a high concentration of BQ inhibited the removal of DCF, because the intermediates generating ¹O₂ were scavenged. For further validation, EPR tests were carried out in the pyrogallol system. The EPR test results (Fig. S17 revealed that the pyrogallol system contained not only a considerable signal of DMPO-O $_2^{ullet}$ but also a clear signal of the TEM- $PO^{-1}O_2$ triplet line. The EPR results proved that O_2^{\bullet} was easily converted to ${}^{1}O_{2}$, so the main contribution of O_{2}^{\bullet} was more likely to serve as an intermediate of ¹O₂. Therefore, we inferred that ¹O₂ was the main RS in the removal of DCF. Previous study reported that only Fe (IV) and •OH were generated in the Fe (VI)/PAA system [79]. Therefore, we employed Fe (VI)/PAA system as the baseline reaction to produce Fe (IV) so as to verify the contribution of Fe (IV) in the removal of DCF. From the Fig. 4c, we obserived that Fe (VI)/PAA can remove DCF obviously. The addition of TBA has little effect on the DCF removal in

the Fe (VI)/PAA system,indicating that the removal of DCF in Fe (VI)/PAA system is due to the presence of Fe (IV) rather than •OH. This result further proved that Fe (IV) was involved in the removal of DCF in the FeS/PAA.

3.4. Assessment of non-radical pathways by the probe-based kinetic model

According to the above conclusions, the removal of DCF in the FeS/ PAA system mainly depended on non-radical pathways. Therefore, we employed a probe-based kinetic model to preliminarily quantify the non-radical pathways (including FeS adsorption, oxidation by PAA, ¹O₂, and Fe (IV)) and evaluate their contributions. The removal of probe contaminants could be emulated by kinetic modeling (Eq. (1)). Based on the decomposition curves of PAA and Eqs. (2) - (3), the exposure of PAA, ¹O₂, and Fe (IV) was obtained (Fig. 5a). The exposure of PAA and $^1\mathrm{O}_2$ increased with the reaction and reached 1.1799 M s and 5.27 imes 10^{-8} M s at 90 min, respectively. Fe (IV) reached its maximum (2.36×10^{-6} M s) at 10 min, and then decreased with the exposure of 1.12×10^{-6} M s at 90 min. The transient concentrations of ¹O₂ and Fe (IV) were determined by using Eqs. (20) - (21) (where R $_{^{1}O_{2}}$ is the ratio of $^{1}O_{2}$ to PAA exposure and $R_{Fe\ (IV)}$ is the ratio of Fe (IV) to PAA exposure) [34]. The transient concentrations of PAA, Fe (IV), and ${}^{1}O_{2}$ were shown in Fig. 5b. The concentration of Fe (IV) was 10^2 – 10^9 times higher than that of 1O_2 . Eventually, based on the exposure of PAA and RS, we calculated the relative contributions of PAA oxidation, ¹O₂ oxidation, Fe (IV) oxidation, and FeS adsorption to DCF removal (f_{PAA} , $f_{^{1}O_{2}}$, $f_{Fe(IV)}$, and f_{ads}) using Eqs. (22) - (25). As shown in Fig. 5c, f_{RS} contributed the most to the DCF removal with 85 %, of which the contribution of ¹O₂ and Fe (IV) was 81.5 % and 3.5 %. The direct oxidation of PAA and FeS adsorption contributed 9.1 % and 5.9 % to DCF removal, respectively.

In general, the results showed that $^1\mathrm{O}_2$ played a dominant role in DCF removal in the FeS/PAA system. Although the exposure of Fe (IV) is greater than that of $^1\mathrm{O}_2$, its contribution to DCF removal is much smaller than that of $^1\mathrm{O}_2$, which is mainly due to the difference in the reactivity of $^1\mathrm{O}_2$ ($k=1.3\times10^{-7}~\mathrm{M}^{-1}~\mathrm{S}^{-1}$) and Fe (IV) ($k=2.51\times10^{-4}~\mathrm{M}^{-1}~\mathrm{S}^{-1}$) to DCF.

$$R_{^{1}O_{2}} = \frac{\int [^{1}O_{2}]dt}{\int [PAA]dt} = \frac{[^{1}O_{2}]}{[PAA]}$$
 (20)

$$R_{Fe(IV)} = \frac{\int \left[Fe(IV)\right]dt}{\int \left[PAA\right]dt} = \frac{\left[Fe(IV)\right]}{\left[PAA\right]} \tag{21} \label{eq:21}$$

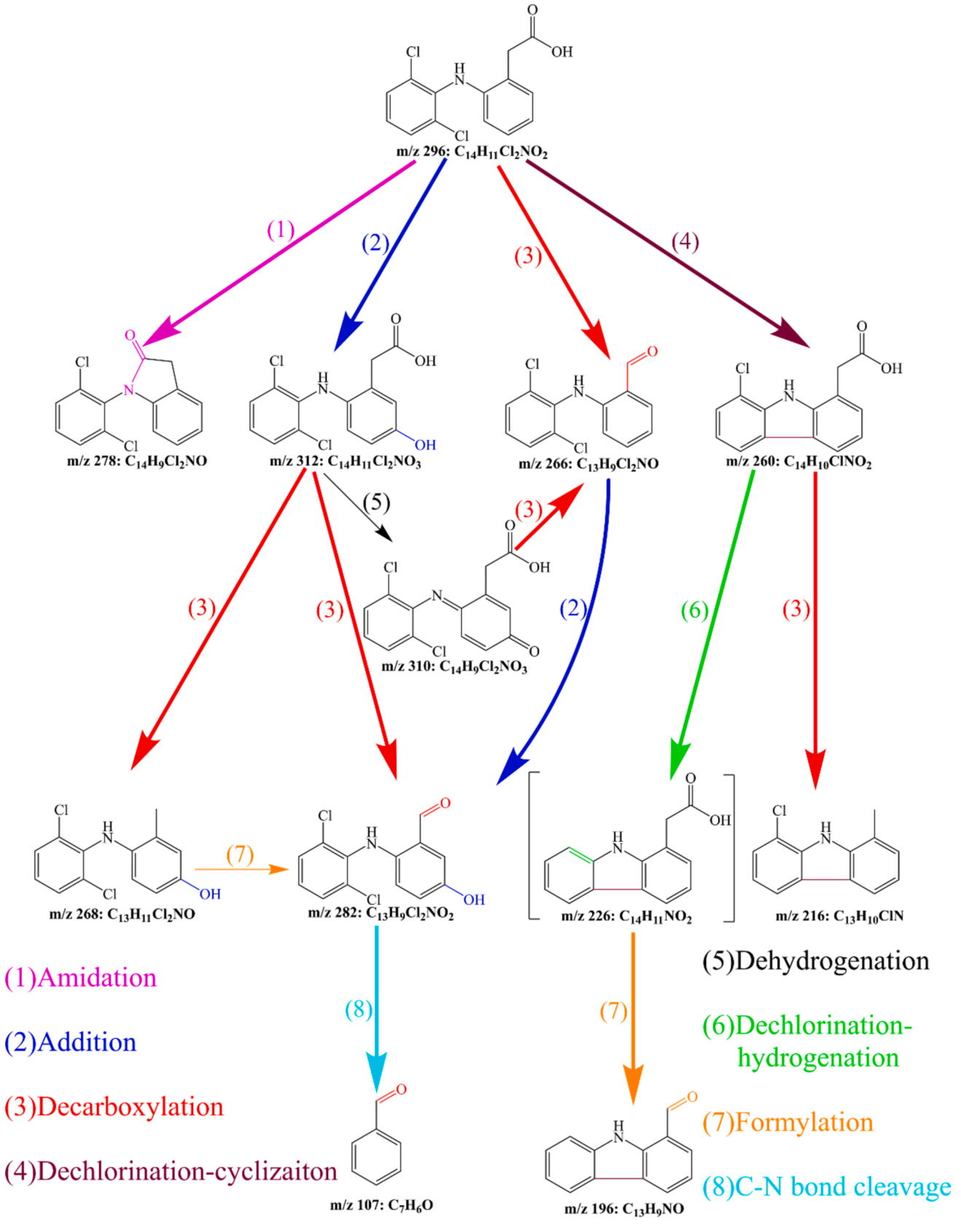


Fig.6. Possible degradation pathways of DCF.

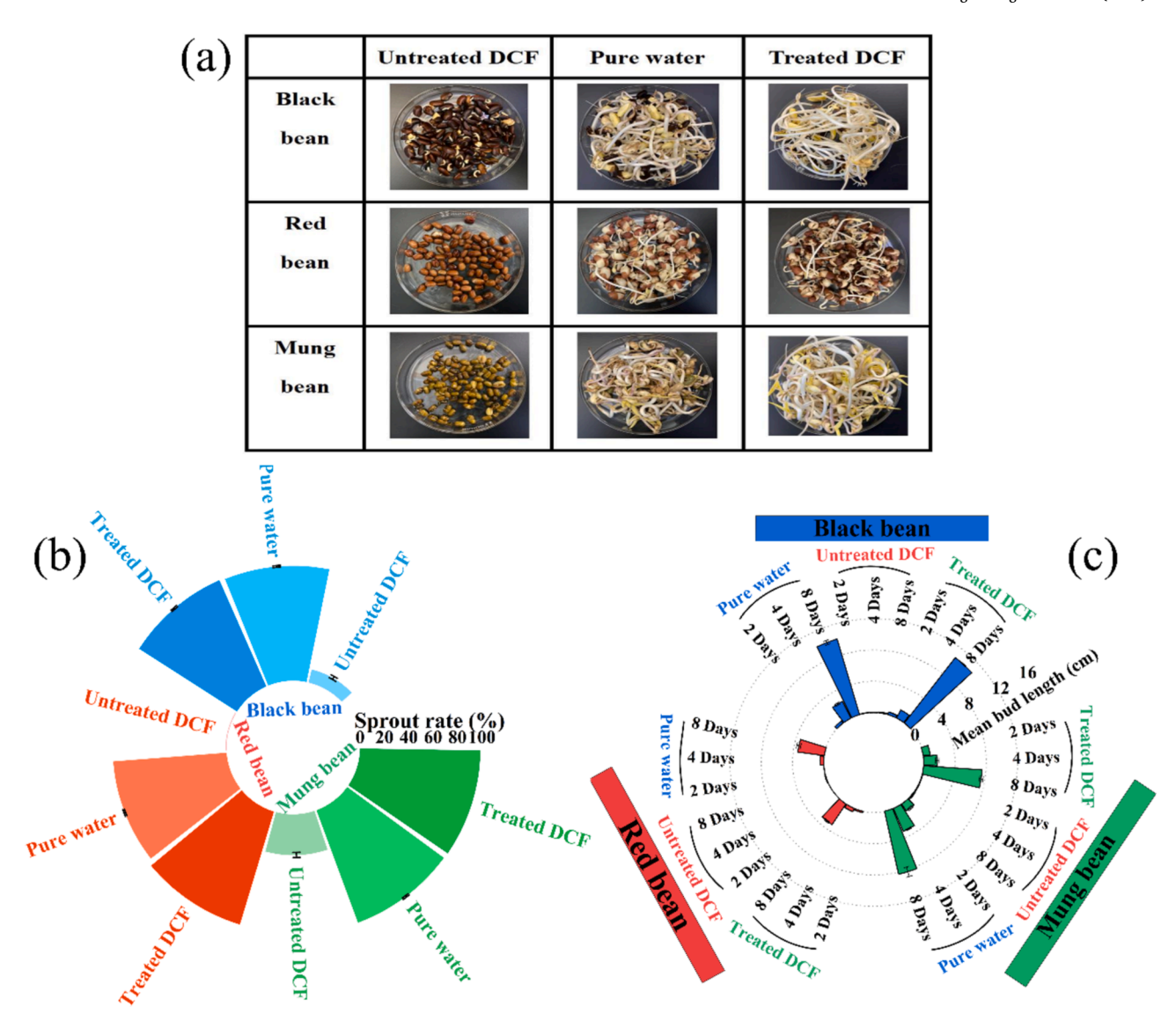


Fig.7. (a) Growth, (b)sprout rate and (c) bud length of black, red, and mung beans after 8 days of incubation in the different solution. (For interpretation of the references to colour in this figure legend, the reader is referred to the web version of this article.)

$$f_{PAA} = \frac{k_{PAA,DCF} \int \left[PAA\right] dt}{k_{PAA,DCF} \int \left[PAA\right] dt + k_{^{1}O_{2},DCF} \int \left[^{1}O_{2}\right] dt + k_{Fe(IV),DCF} \int \left[Fe(IV)\right] dt + k_{ads,DCF} t} \tag{22} \label{eq:22}$$

$$f_{1_{O_{2}}} = \frac{k_{1_{O_{2},DCF}} \int [\,^{1}O_{2}]dt}{k_{PAA,DCF} \int [\,^{1}PAA]dt + k_{1_{O_{2},DCF}} \int [\,^{1}O_{2}]dt + k_{Fe(IV),DCF} \int [Fe(IV)\,]dt + k_{ads,def}t} \tag{23}$$

$$f_{Fe(IV)} = \frac{k_{Fe(IV),DCF} \int \left[Fe(IV)\right] dt}{k_{PAA,DCF} \int \left[PAA\right] dt + k_{{}^{1}O_{2},DCF} \int \left[{}^{1}O_{2}\right] dt + k_{Fe(IV),DCF} \int \left[Fe(IV)\right] dt + k_{ads,DCF} t} \tag{24} \label{eq:fe(IV)}$$

$$f_{ads} = \frac{k_{ads,DCF}t}{k_{PAA,DCF}\int \left[PAA\right]dt + k_{^{1}O_{2},DCF}\int \left[^{1}O_{2}\right]dt + k_{Fe(IV),DCF}\int \left[Fe(IV)\right]dt + k_{ads,DCF}t} \tag{25} \label{eq:25}$$

3.5. Degradation pathway of DCF and the toxicity of its degradation products

Ten degradation products of DCF were detected with UPLC-Q-TOF-

MS, Fig. S18 shows the mass spectra and chromatograms of each degradation product. The possible degradation pathways were presented in Fig. 6. As we can see, amidation, addition, decarboxylation, dechlorination-cyclization, dehydrogenation, dechlorination-hydrogenation, formylation, and C-N bond cleavage were involved in the DCF degradation. (1) Amidation: The amidation reaction can be

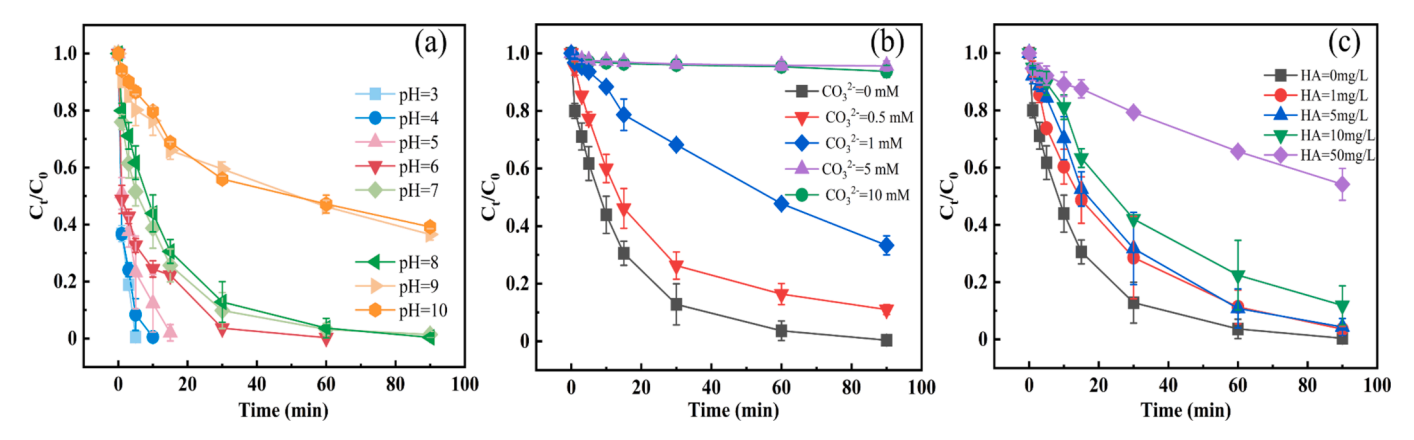


Fig. 8. Effect of (a) pH, (b) CO₃², (c) HA on the removal of DCF in the FeS/PAA system. Conditions: [DCF] = 1 mg/L, [FeS] = 100 mg/L, [PAA] = 500 μM.

viewed as substituting a hydroxy group in the carboxyl group with an amino group. The amidation may be facilitated by the existence of both carboxyl and sec-amino groups in the DCF molecular structure, thereby promoting the production of m/z 278 [80,81]. (2) Addition: The atoms in the DCF with a larger density of electron clouds were attacked [82], initiating an addition reaction to produce m/z 312 and m/z 282 [83]. (3) Decarboxylation: Decarboxylation means the shedding of the carboxyl group from the acetate group of the DCF molecule. The generation of *m*/ z 266 can be attributed to the decarboxylation of DCF, which was detected in the degradation of DCF by Fe (VI) [84], implying that Fe(IV) may also be involved in the decarboxylation of DCF. (4) Dechlorinationcyclizations: after the C-Cl bond cleavage of the DCF, the formation of the C-cations and the intramolecular electron transfer of DCF, which may be caused by ¹O₂, ultimately led to the formation of the cyclization product m/z 260.(5) Dehydrogenation: the phenol and aniline groups of m/z 312 are electron-rich groups and can be dehydrogenated to produce m/z 310 [83]. (6) Dechlorination-hydrogenation: the chlorine atom in the DCF benzene ring was replaced with a hydrogen atom. m/z 226 may be further produced from m/z 260. Although this product was not detectable in the study, it is a necessary ingredient for the formation of the m/z 196 product [80]. (7) Formylation: a reaction in which an aldehyde group is introduced. m/z 268 and m/z 226 may be formulated by electrophilic attack [84,85]. (8) C-N bond cleavage: ¹O₂ or Fe (IV) may attack the C-N bond between the two aromatic rings of DCF, which in turn generates the cleavage product m/z 107 [84,86].

We further assessed the toxicity of DCF degradation products by analyzing the sprout rate and mean bud length of each of the three types of beans. Mung, red, and black beans, as typical legumes, are characterized by non-harsh sprouting conditions and rapid growth, which facilitates the elimination of interferences and the efficient carrying out of phytotoxicity analyses. As shown in Fig. 7a and b, untreated DCF greatly reduced the sprout rate of the three types of beans, while the sprout rates of the treated DCF (DCF degradation products) system and the pure water system were virtually the same, proving that the toxicity of the degradation products of DCF was dramatically reduced. In the mean bud length test (Fig. 7a and c), untreated DCF showed considerable inhibition of mean bud length, and the mean bud length difference between the treated DCF system and the pure water system was within 0.8 cm (eight days). In order to exclude the possible interference of acetic acid in PAA solution as a carbon source, we also explored the effects of pure water system containing acetic acid and DCF solution containing acetic acid on the mean bud length and sprout rate of the three types of beans, respectively. The results (Fig. S19 (a-b)) showed that acetic acid in PAA hardly affected bean growth. The mean bud length of black beans in the treated DCF system (10.6 cm) was longer than that in the pure water system (10.1 cm), most likely due to the PAA's organic content, which would slightly promote plant growth. The sprout rate and mean bud length tests indicated that the toxicity of the DCF products was dramatically reduced in the FeS/PAA system. From the application perspective, we also analyzed the effect of the FeS/PAA system on bean sprout rate and mean bud length when DCF was not added. The results showed (Fig. S19(c)) that there was almost no adverse effect of the FeS/PAA system on bean sprout rate or mean bud length, which affirmed the excellent environmental friendliness and wide application prospect of the FeS/PAA system.

The potential toxicity of DCF and DCF degradation intermediates was further predicted by the ECOSAR program based on quantitative structure–activity relationship (QSAR). As shown in Table S3, the acute and chronic toxicity of some of the intermediates were reduced, such as m/z 312, m/z 260, and m/z 310, which demonstrated the prospects of the FeS/PAA system in reducing the toxicity of DCF. It is noteworthy that the acute and chronic toxicity of some of the intermediates were even higher than that of the DCF parent, such as m/z 266, m/z 216, m/z 107, and m/z 196, among which m/z 216 had a chronic toxicity rating of "Very toxic" to fish, daphnid, and green algae. Therefore, the potential risk of intermediates in the degradation of DCF based on AOPs needs to be further investigated.

3.6. Effect of pH, anions, and humic acid on DCF removal

3.6.1. pH

Because pH affects the generation and activity of RS, pH is usually a determining factor affecting AOPs [79,87]. As shown in Fig. 8a, different initial pH had an influence on DCF removal. On the other hand, Fig. S20 showed almost no changes in pH during the reaction. The removal of DCF by the FeS/PAA system can reach 98 % in the initial pH range of 3 to 8. The faster reaction rate for DCF removal under acidic condition (Fig. S21) was attributed to acidic condition, and the homogeneous Fe (II) activation of PAA became the dominant way to synergistically remove DCF by generating •OH, R-O•, etc [19,80,88]. However, the faster DCF removal under acidic conditions is not favorable for practical application in environmental water bodies, which are mostly nearly neutral. At an alkaline pH (pH = 9-10), more than 60 % of DCF removal was still achieved at 90 min. However, the reaction rate dropped under alkaline condition (Fig. S21), which may be attributed to the deprotonated PAA (PAA⁻) with weak oxidizing ability as the predominant form [9] and the formation of iron hydroxide complexes under alkaline conditions [19].

3.6.2. Anions

Since anions in the water body could have a scavenging impact on free radicals [89], it could impact the degradation of organic pollutants by AOPs. $^{1}O_{2}$, as a non-radical RS, is unaffected by anions [78,90]. Therefore, Cl $^{-}$, SO $_{4}^{2}$, and NO $_{3}^{-}$ hardly affected the removal of DCF (Fig. S22). The presence of HCO $_{3}^{2}$ $^{-}$ slightly slowed down DCF removal in the middle of the reaction, and the reason may be that HCO $_{3}^{-}$ scavenged

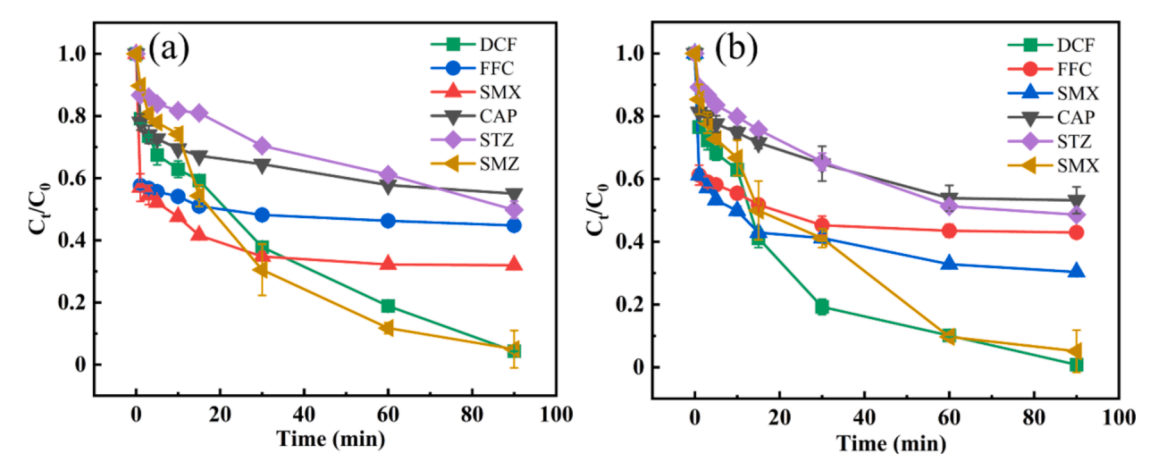


Fig.9. Removal of multiple pharmaceuticals by FeS/PAA (a: ultrapure water sample. b: real water sample). Conditions: [individual pharmaceuticals] = 1 mg/L, [FeS] = 300 mg/L, [PAA] = 2 mM.

some O_2^{\bullet} , but at the termination of the reaction, DCF removal was almost unaffected (Fig. S23). Notably, CO_3^2 exhibited inhibition of DCF removal, and the degree of inhibition increased as the CO_3^{2-} concentration increased (Fig. 8b). We hypothesized that CO₃²⁻ hydrolysis (Eq. 26) produced a large amount of OH-, which increased the pH in the system and thus inhibited the removal of DCF. We monitored the pH variation when CO_3^{2-} was present, and the results showed (Fig. S24) that the pH in the system was indeed raised. To further verify this speculation, we added 0.1 M H₂SO₄ to the reaction system at 10 min to adjust the pH in the reaction and continued to monitor the DCF removal. The results (Fig. S25) indicated that the removal of DCF and the reaction rate constant were enhanced by the addition of H2SO4. Indirectly, it was demonstrated that CO₃²⁻ inhibits DCF removal, mainly due to the hydrolysis of CO₃²⁻ to produce OH⁻ which raised the pH of the reaction system. Additionally, CO_3^{2-} may scavenge $O_2^{\bullet -}$ (k = 5.0 × 10⁸ M⁻¹ S⁻¹) [91] and produce less reactive CO₃ - radicals [92], thus inhibiting the formation of ${}^{1}O_{2}$.

$$CO_3^{2-} + H_2O \rightleftharpoons HCO_3^{-} + OH^{-}$$
 (26)

3.6.3. Humic acid

Fig. 8c showed that the existence of humic acid (HA) inhibited the removal of DCF more significantly, especially when the HA concentration was higher (50 mg/L), the DCF removal decreased to 45.87 %. The inhibition effect of HA may be caused by the HA chelating the Fe element in the system, resulting in a reduction of effective FeS for activating PAA. Therefore, we further introduced an extra amount of FeS at 5 min of the reaction and continued to monitor the removal of DCF (Fig. S26). The results illustrated that the DCF removal and the reaction rate constant increased significantly when FeS was additionally added. This was further verified that HA with high concentration chelated the Fe element, thus inhibiting the removal of DCF. In addition, the competitive consumption of $^1\mathrm{O}_2$ in the system by HA may also be responsible for affecting DCF removal [93].

3.7. Recyclability of FeS and adaptability of FeS /PAA system for removing multiple pharmaceuticals in real water samples

One of the advantages of non-homogeneous activation over homogeneous activation is a certain capacity for reuse. As shown in Fig. S27, 99.6 % of DCF could be degraded by the fresh FeS/PAA system, and the removal of DCF decreased to 80 % after the first cycle. After reusing FeS for 4 times, the removed DCF still achieved 51.5 % within 90 min. This indicated that FeS still maintained better catalytic activity after reuse.

To examine the effectiveness of the FeS/PAA system in practical

applications, multiple pharmaceuticals coexistence systems and real water samples (surface water) were employed. Six different kinds of pharmaceuticals including DCF, florfenicol (FFC), sulfamethoxazole (SMX), chloramphenicol (CAP), sulfathiazole (STZ), and sulfamethazine (SMZ) were selected as target pollutants. Apart from DCF, the other five pharmaceuticals are representative antibiotics that were difficult to degrade and potentially risky [36,94-97]. As shown in Fig. 9a, FeS/PAA system showed good removal ability for DCF, FFC, SMX, CAP, STZ, and SMZ, and their removal within 90 min were 95.7 %, 55.3 %, 68.1 %, 45.1 %, 50.2 %, and 95.1 %, respectively. This indicated that the FeS/ PAA system is a highly efficient technology for the removal of various pharmaceuticals. Compared to the ultrapure water sample, the removal of six pharmaceuticals in real water had no obvious difference (Fig. 9b), which further demonstrated the compatibility of the ¹O₂-based FeS/PAA system in real water bodies. In conclusion, the FeS/PAA system exhibited good anti-interference performance towards the real water matrix and possessed potential applications for removing pharmaceuticals in water treatment.

4. Conclusions

This study used natural FeS to activate PAA for efficient removal of DCF from water under near-neutral conditions. The results showed that commercial FeS could activate PAA and the main contribution to DCF removal was ¹O₂. The FeS/PAA system exhibited excellent performance in a wide pH range (3-8). The FeS/PAA system achieved high DCF removal in 90 min with $k_{\rm obs}$ of 0.0582 min⁻¹. The existence of the anions Cl⁻, SO₄²⁻, NO₃, and HCO₃ had almost no influence on the removal of DCF dominated by non-radical oxidation. HA with a high concentration (50 mg/L) could chelate the Fe element, thus inhibiting the removal of DCF. The inhibitory effect of CO_3^{2-} was due to the alkaline environment resulting from its hydrolysis. The multi-pharmaceutical coexistence system and its application in real water bodies proved that the FeS/PAA system has excellent anti-disturbance and decontamination ability. The analysis of DCF intermediates and phytotoxicity tests showed that the toxicity of DCF treated by the FeS/PAA system was significantly reduced. The FeS/PAA system would have good potential in the removal of pharmaceuticals in actual water bodies. To sum up, this study not only thoroughly investigated the FeS/PAA system to remove micropollutants from water by non-radical pathway under near-neutral condition, which supports the application of AOPs based on activated PAA, but also provides further exploration on the multiple identification and contribution of RS, which provided a reference for in-depth understanding the mechanism of AOPs based on activated PAA.

CRediT authorship contribution statement

Yao-Feng Gao: Writing – original draft, Methodology, Investigation, Formal analysis, Data curation. Yan-Ping Duan: Writing – review & editing, Supervision, Project administration, Methodology, Data curation, Conceptualization. Yu-Ru Chen: Visualization, Software, Data curation. Yuan-Hua Jia: Writing – review & editing, Data curation. Yao-Jen Tu: Investigation, Data curation. Chao-Meng Dai: Methodology, Investigation, Funding acquisition, Conceptualization.

Declaration of competing interest

The authors declare that they have no known competing financial interests or personal relationships that could have appeared to influence the work reported in this paper.

Acknowledgments

This study was funded by the National Natural Science Foundation of China (42077175), Shanghai "Science and Technology Innovation Action Plan" Project (21230712100).

Appendix A. Supplementary data

Supplementary data to this article can be found online at https://doi.org/10.1016/j.cej.2024.158071.

Data availability

I have shared the link to my data at the Attach File step.

References

- G. Orive, U. Lertxundi, T. Brodin, P. Manning, Greening the pharmacy, Science 377 (6603) (2022) 259–260, https://doi.org/10.1126/science.abp9554.
- [2] S.C. Wiles, M.G. Bertram, J.M. Martin, H. Tan, T.K. Lehtonen, B.B.M. Wong, Long-term pharmaceutical contamination and temperature stress disrupt fish behavior, Environ. Sci. Tech. 54 (13) (2020) 8072–8082, https://doi.org/10.1021/acs.est/0.01625
- [3] D. Kötke, J. Gandrass, Z. Xie, R. Ebinghaus, Prioritised pharmaceuticals in German estuaries and coastal waters: occurrence and environmental risk assessment, Environ. Pollut. 255 (2019) 113161, https://doi.org/10.1016/j. envirol. 2010.113161
- [4] C. Cannata, T. Backhaus, I. Bramke, M. Caraman, A. Lombardo, R. Whomsley, C.T. A. Moermond, A.M.J. Ragas, Prioritisation of data-poor pharmaceuticals for empirical testing and environmental risk assessment, Environ. Int. 183 (2024) 108379, https://doi.org/10.1016/j.envint.2023.108379.
- [5] C. Matthee, A.R. Brown, A. Lange, C.R. Tyler, Factors determining the susceptibility of fish to effects of human pharmaceuticals, Environ. Sci. Tech. 57 (24) (2023) 8845–8862, https://doi.org/10.1021/acs.est.2c09576.
- [6] Y.-R. Chen, Y.-P. Duan, Z.-B. Zhang, Y.-F. Gao, C.-M. Dai, Y.-J. Tu, J. Gao, Comprehensive evaluation of antibiotics pollution the Yangtze River basin, China: emission, multimedia fate and risk assessment, J. Hazard. Mater. 465 (2024) 133247, https://doi.org/10.1016/j.jhazmat.2023.133247.
- [7] J.L. Oaks, M. Gilbert, M.Z. Virani, R.T. Watson, C.U. Meteyer, B.A. Rideout, H. L. Shivaprasad, S. Ahmed, M.J. Iqbal Chaudhry, M. Arshad, S. Mahmood, A. Ali, A. Ahmed Khan, Diclofenac residues as the cause of vulture population decline in Pakistan, Nature 427 (6975) (2004) 630–633, https://doi.org/10.1038/patire0/2317
- [8] R. Triebskorn, H. Casper, A. Heyd, R. Eikemper, H.R. Köhler, J. Schwaiger, Toxic effects of the non-steroidal anti-inflammatory drug diclofenae: part II. Cytological effects in liver, kidney, gills and intestine of rainbow trout (Oncorhynchus mykiss), Aquat. Toxicol. 68 (2) (2004) 151–166, https://doi.org/10.1016/j.aquatox.2004.03.015.
- [9] J. Kim, C.-H. Huang, Reactivity of peracetic acid with organic compounds: a critical review, ACS ES&T Water 1 (1) (2021) 15–33, https://doi.org/10.1021/ acsestwater.0c00029.
- [10] L. An, X. Kong, M. Jiang, W. Li, Q. Lv, X. Hou, C. Liu, P. Su, J. Ma, T. Yang, Photo-assisted natural chalcopyrite activated peracetic acid for efficient micropollutant degradation, Water Res. 257 (2024) 121699, https://doi.org/10.1016/j.watres.2024.121699.
- [11] X. Niu, J. Wei, Z. Jiang, X. Cui, Y. Li, N. Cui, J. Li, L. Wang, J. Huo, W. Ji, X. Zhang, J. Li, New insights into the pH-dependent removal of sulfamethoxazole in peracetic acid activation systems: from mechanistic exploration to practical application potentials, J. Hazard. Mater. 474 (2024) 134674, https://doi.org/10.1016/j.jhazmat.2024.134674.

- [12] Y. Dong, C.-S. He, S. Sun, J. Liu, Z.-H. Xie, J.-Y. Li, P. Zhou, H. Zhang, F. Dong, B. Lai, Mechanically treated Mn₂O₃ triggers peracetic acid activation for superior non-radical oxidation of micropollutants: identification of reactive complexes, Water Res. 255 (2024) 121486, https://doi.org/10.1016/j.watres.2024.121486.
- [13] X. Ao, W. Wang, W. Sun, Z. Lu, C. Li, Degradation and transformation of norfloxacin in medium-pressure ultraviolet/peracetic acid process: an investigation of the role of pH, Water Res. 203 (2021) 117458, https://doi.org/10.1016/j. water 2021 117458
- [14] J. Wang, Y. Wan, J. Ding, Z. Wang, J. Ma, P. Xie, M.R. Wiesner, Thermal activation of peracetic acid in aquatic solution: the mechanism and application to degrade sulfamethoxazole, Environ. Sci. Tech. 54 (22) (2020) 14635–14645, https://doi. org/10.1021/acs.est.0c02061.
- [15] D. Kiejza, U. Kotowska, W. Polińska, J. Karpińska, Peracids New oxidants in advanced oxidation processes: the use of peracetic acid, peroxymonosulfate, and persulfate salts in the removal of organic micropollutants of emerging concern – A review, Sci. Total Environ. 790 (2021) 148195, https://doi.org/10.1016/j. scitoteny 2021 148195
- [16] T. Luukkonen, U. von Gunten, Oxidation of organic micropollutant surrogate functional groups with peracetic acid activated by aqueous Co(II), Cu(II), or Ag(I) and geopolymer-supported Co(II), Water Res. 223 (2022) 118984, https://doi.org/ 10.1016/j.watres.2022.118984.
- [17] R. Zhou, G. Zhou, Y. Liu, S. Liu, S. Wang, Y. Fu, Activated peracetic acid by Mn3O4 for sulfamethoxazole degradation: a novel heterogeneous advanced oxidation process, Chemosphere 306 (2022) 135506, https://doi.org/10.1016/j. chemosphere.2022.135506.
- [18] Z. Zhang, Y. Duan, C. Dai, S. Li, Y. Chen, Y. Tu, K.H. Leong, L. Zhou, Oxidation of sulfamethazine by peracetic acid activated with biochar: reactive oxygen species contribution and toxicity change, Environ. Pollut. 313 (2022) 120170, https://doi. org/10.1016/j.envpol.2022.120170.
- [19] J. Kim, T. Zhang, W. Liu, P. Du, J.T. Dobson, C.-H. Huang, Advanced oxidation process with peracetic acid and Fe(II) for contaminant degradation, Environ. Sci. Tech. 53 (22) (2019) 13312–13322, https://doi.org/10.1021/acs.est.9b02991.
- [20] D. Xing, S. Shao, Y. Yang, Z. Zhou, G. Jing, X. Zhao, Mechanistic insights into the efficient activation of peracetic acid by pyrite for the tetracycline abatement, Water Res. 222 (2022) 118930, https://doi.org/10.1016/j.watres.2022.118930.
- [21] D. Cheng, S. Yuan, P. Liao, P. Zhang, Oxidizing impact induced by mackinawite (FeS) nanoparticles at oxic conditions due to production of hydroxyl radicals, Environ. Sci. Tech. 50 (21) (2016) 11646–11653, https://doi.org/10.1021/acs. est 6b02833
- [22] H. Chen, Z. Zhang, M. Feng, W. Liu, W. Wang, Q. Yang, Y. Hu, Degradation of 2,4-dichlorophenoxyacetic acid in water by persulfate activated with FeS (mackinawite), Chem. Eng. J. 313 (2017) 498–507, https://doi.org/10.1016/j.cei.2016.12.075.
- [23] D. Cheng, A. Neumann, S. Yuan, W. Liao, A. Qian, Oxidative degradation of organic contaminants by FeS in the presence of O₂, Environ. Sci. Tech. 54 (7) (2020) 4091–4101, https://doi.org/10.1021/acs.est.9b07012.
- [24] L. Wang, J. Wei, Y. Li, J. Huo, W. Ji, N. Cui, J. Li, X. Niu, Z. Jiang, X. Cui, J. Li, A state-of-the-art review on heterogeneous catalysts-mediated activation of peracetic acid for micropollutants degradation: classification of reaction pathways, mechanisms, influencing factors and DFT calculation, Chem. Eng. J. 477 (2023) 147051, https://doi.org/10.1016/j.cej.2023.147051.
- [25] L. Zhang, J. Chen, T. Zheng, Y. Xu, T. Liu, W. Yin, Y. Zhang, X. Zhou, Co–Mn spinel oxides trigger peracetic acid activation for ultrafast degradation of sulfonamide antibiotics: unveiling critical role of Mn species in boosting Co activity, Water Res. 229 (2023) 119462, https://doi.org/10.1016/j.watres.2022.119462.
- [26] J. Wu, Y. Wang, Z. Yu, D. Wei, D. Li, C. Wen, P. Chen, H. Liu, W. Lv, G. Liu, Efficient activation of peracetic acid via a defect-rich carbon nanotube@Co₃O₄ three-dimensional network for antibiotic removal: mechanism insights and practical water remediation, Environ. Sci. Nano 10 (2) (2023) 528–538, https://doi.org/10.1039/D2EN01088G.
- [27] S.-R. Yang, C.-S. He, Z.-H. Xie, L.-L. Li, Z.-K. Xiong, H. Zhang, P. Zhou, F. Jiang, Y. Mu, B. Lai, Efficient activation of PAA by FeS for fast removal of pharmaceuticals: the dual role of sulfur species in regulating the reactive oxidized species, Water Res. 217 (2022) 118402, https://doi.org/10.1016/j.watres.2022.118402.
- [28] S. Li, C. Dai, Y. Duan, Z. Li, Z. Zhang, X. Lai, J. Li, J. Hu, L. Zhou, Y. Zhang, S. Liu, R. Fu, Non-radical pathways in peracetic acid-based micropollutant degradation: a comprehensive review of mechanisms, detection methods, and promising applications, Sep. Purif. Technol. 330 (2024) 125240, https://doi.org/10.1016/j.seppur.2023.125240.
- [29] Y. Yao, C. Wang, X. Yan, H. Zhang, C. Xiao, J. Qi, Z. Zhu, Y. Zhou, X. Sun, X. Duan, J. Li, Rational regulation of Co–N–C coordination for high-efficiency generation of ¹O₂ toward nearly 100% selective degradation of organic pollutants, Environ. Sci. Tech. 56 (12) (2022) 8833–8843, https://doi.org/10.1021/acs.est.2c00706.
- [30] A.A. Frimer, The reaction of singlet oxygen with olefins: the question of mechanism, Chem. Rev. 79 (5) (1979) 359–387, https://doi.org/10.1021/ cr60321a001
- [31] Y. Wang, Y. Lin, S. He, S. Wu, C. Yang, Singlet oxygen: properties, generation, detection, and environmental applications, J. Hazard. Mater. 461 (2024) 132538, https://doi.org/10.1016/j.jhazmat.2023.132538.
- [32] Q. Fang, H. Yang, S. Ye, P. Zhang, M. Dai, X. Hu, Y. Gu, X. Tan, Generation and identification of ¹O₂ in catalysts/peroxymonosulfate systems for water purification, Water Res. 245 (2023) 120614, https://doi.org/10.1016/j.watres.2023.120614.
- [33] Y. Zong, L. Chen, Y. Zeng, J. Xu, H. Zhang, X. Zhang, W. Liu, D. Wu, Do we appropriately detect and understand singlet oxygen possibly generated in

- advanced oxidation processes by electron paramagnetic resonance spectroscopy? Environ. Sci. Tech. 57 (25) (2023) 9394–9404, https://doi.org/10.1021/acs.est 3c01553
- [34] H. Wang, L. Gao, Y. Xie, G. Yu, Y. Wang, Clarification of the role of singlet oxygen for pollutant abatement during persulfate-based advanced oxidation processes: Co₃O₄@CNTs activated peroxymonosulfate as an example, Water Res. 244 (2023) 120480, https://doi.org/10.1016/j.watres.2023.120480.
- [35] E. Zhu, D. Yuan, Z. Wang, Q. Zhang, S. Tang, Insight into the activation mechanism of peracetic acid by molybdenum carbide for sulfamethoxazole decomposition, Chem. Eng. J. 474 (2023) 145824, https://doi.org/10.1016/j.cej.2023.145824.
- [36] C. Dai, S. Li, Y. Duan, K.H. Leong, S. Liu, Y. Zhang, L. Zhou, Y. Tu, Mechanisms and product toxicity of activated carbon/peracetic acid for degradation of sulfamethoxazole: implications for groundwater remediation, Water Res. 216 (2022) 118347, https://doi.org/10.1016/j.watres.2022.118347.
- [37] J. Xiao, M. Wang, Z. Pang, L. Dai, J. Lu, J. Zou, Simultaneous spectrophotometric determination of peracetic acid and the coexistent hydrogen peroxide using potassium iodide as the indicator, Anal. Methods 11 (14) (2019) 1930–1938, https://doi.org/10.1039/C8AY02772B.
- [38] L. Gao, Y. Guo, J. Zhan, G. Yu, Y. Wang, Assessment of the validity of the quenching method for evaluating the role of reactive species in pollutant abatement during the persulfate-based process, Water Res. 221 (2022) 118730, https://doi.org/10.1016/j.watres.2022.118730.
- [39] Y. Guo, J. Long, J. Huang, G. Yu, Y. Wang, Can the commonly used quenching method really evaluate the role of reactive oxygen species in pollutant abatement during catalytic ozonation? Water Res. 215 (2022) 118275 https://doi.org/ 10.1016/j.watres.2022.118275.
- [40] F. Wilkinson, W.P. Helman, A.B. Ross, Rate constants for the decay and reactions of the lowest electronically excited singlet state of molecular oxygen in solution. an expanded and revised compilation, J. Phys. Chem. Ref. Data 24 (2) (1995) 663–677, https://doi.org/10.1063/1.555965.
- [41] O. Pestovsky, A. Bakac, Aqueous Ferryl(IV) ion: kinetics of oxygen atom transfer to substrates and oxo exchange with solvent water, Inorg. Chem. 45 (2) (2006) 814–820, https://doi.org/10.1021/ic051868z.
- [42] M. Wolthers, S.J. Van Der Gaast, D. Rickard, The structure of disordered mackinawite, Am. Mineral. 88 (11–12) (2003) 2007–2015, https://doi.org/ 10.2138/am-2003-11-1245.
- [43] A.D. Bokare, W. Choi, Review of iron-free Fenton-like systems for activating H₂O₂ in advanced oxidation processes, J. Hazard. Mater. 275 (2014) 121–135, https://doi.org/10.1016/j.jhazmat.2014.04.054.
- [44] X. Ling, A. Cai, M. Chen, H. Sun, S. Xu, Z. Huang, X. Li, J. Deng, A comparison of oxidation and re-flocculation behaviors of Fe²⁺/PAA and Fe²⁺/H₂O₂ treatments for enhancing sludge dewatering: a mechanism study, Sci. Total Environ. 847 (2022) 157690. https://doi.org/10.1016/j.scitoteny.2022.157690.
- [45] T.D. Carlos, L.B. Bezerra, M.M. Vieira, R.A. Sarmento, D.H. Pereira, G.S. Cavallini, Fenton-type process using peracetic acid: efficiency, reaction elucidations and ecotoxicity, J. Hazard. Mater. 403 (2021) 123949, https://doi.org/10.1016/j. jhazmat.2020.123949.
- [46] Y. Zhou, X. Wang, C. Zhu, D.D. Dionysiou, G. Zhao, G. Fang, D. Zhou, New insight into the mechanism of peroxymonosulfate activation by sulfur-containing minerals: role of sulfur conversion in sulfate radical generation, Water Res. 142 (2018) 208–216, https://doi.org/10.1016/j.watres.2018.06.002.
- [47] J. Fan, L. Gu, D. Wu, Z. Liu, Mackinawite (FeS) activation of persulfate for the degradation of p-chloroaniline: surface reaction mechanism and sulfur-mediated cycling of iron species, Chem. Eng. J. 333 (2018) 657–664, https://doi.org/ 10.1016/j.cej.2017.09.175
- [48] A. Ghauch, H. Abou Assi, S. Bdeir, Aqueous removal of diclofenac by plated elemental iron: bimetallic systems, J. Hazard. Mater. 182 (1) (2010) 64–74, https://doi.org/10.1016/j.jhazmat.2010.05.139.
- [49] M. Cai, P. Sun, L. Zhang, C.-H. Huang, UV/peracetic acid for degradation of pharmaceuticals and reactive species evaluation, Environ. Sci. Tech. 51 (24) (2017) 14217–14224, https://doi.org/10.1021/acs.est.7b04694.
- [50] L. Meng, J. Dong, J. Chen, L. Li, Q. Huang, J. Lu, Activation of peracetic acid by spinel FeCo₂O₄ nanoparticles for the degradation of sulfamethoxazole, Chem. Eng. J. 456 (2023) 141084, https://doi.org/10.1016/j.cej.2022.141084.
- [51] C. Qi, X. Liu, J. Ma, C. Lin, X. Li, H. Zhang, Activation of peroxymonosulfate by base: Implications for the degradation of organic pollutants, Chemosphere 151 (2016) 280–288, https://doi.org/10.1016/j.chemosphere.2016.02.089.
- [52] J. Kim, P. Du, W. Liu, C. Luo, H. Zhao, C.-H. Huang, Cobalt/peracetic acid: advanced oxidation of aromatic organic compounds by acetylperoxyl radicals, Environ. Sci. Tech. 54 (8) (2020) 5268–5278, https://doi.org/10.1021/acs. est.0c00356.
- [53] M.L. Fork, J.B. Fick, A.J. Reisinger, E.J. Rosi, Dosing the coast: leaking sewage infrastructure delivers large annual doses and dynamic mixtures of pharmaceuticals to urban rivers, Environ. Sci. Tech. 55 (17) (2021) 11637–11645, https://doi.org/10.1021/acs.est.1c00379.
- [54] T.-K. Kim, D.L. Sedlak, Mineralization of a fully halogenated organic compound by persulfate under conditions relevant to in situ reduction and oxidation: reduction of hexachloroethane by ethanol addition followed by oxidation, Environ. Sci. Tech. 57 (36) (2023) 13691–13698, https://doi.org/10.1021/acs.est.3c03489.
- [55] H. Dong, Y. Li, S. Wang, W. Liu, G. Zhou, Y. Xie, X. Guan, Both Fe(IV) and radicals are active oxidants in the Fe(II)/peroxydisulfate process, Environ. Sci. Technol. Lett. 7 (3) (2020) 219–224, https://doi.org/10.1021/acs.estlett.0c00025.
- [56] F. Jacobsen, J. Holcman, K. Sehested, Reactions of the ferryl ion with some compounds found in cloud water, Int. J. Chem. Kinet. 30 (3) (1998) 215–221, https://doi.org/10.1002/(SICI)1097-4601(1998)30:3<215::AID-KIN7>3.0.CO;2-V.

- [57] J. He, X. Yang, B. Men, D. Wang, Interfacial mechanisms of heterogeneous Fenton reactions catalyzed by iron-based materials: a review, J. Environ. Sci. 39 (2016) 97–109, https://doi.org/10.1016/j.jes.2015.12.003.
- [58] W.R. Haag, J.R. Hoigne, E. Gassman, A.M. Braun, Singlet oxygen in surface waters — Part I: furfuryl alcohol as a trapping agent, Chemosphere 13 (5) (1984) 631–640, https://doi.org/10.1016/0045-6535(84)90199-1.
- [59] J.R. Hurst, G.B. Schuster, Nonradiative relaxation of singlet oxygen in solution, J. Am. Chem. Soc. 105 (18) (1983) 5756–5760, https://doi.org/10.1021/ ia00356a009.
- [60] W.R. Haag, J. Hoigne, Singlet oxygen in surface waters. 3. Photochemical formation and steady-state concentrations in various types of waters, Environ. Sci. Technol. 20 (4) (1986) 341–348, https://doi.org/10.1021/es00146a005.
- [61] P. Duan, Y. Qi, S. Feng, X. Peng, W. Wang, Y. Yue, Y. Shang, Y. Li, B. Gao, X. Xu, Enhanced degradation of clothianidin in peroxymonosulfate/catalyst system via core-shell FeMn @ N-C and phosphate surrounding, Appl. Catal. B 267 (2020) 118717, https://doi.org/10.1016/j.apcatb.2020.118717.
- [62] J. Lee, U. von Gunten, J.-H. Kim, Persulfate-based advanced oxidation: critical assessment of opportunities and roadblocks, Environ. Sci. Tech. 54 (6) (2020) 3064–3081, https://doi.org/10.1021/acs.est.9b07082.
- [63] Y. Zhao, M. Sun, X. Wang, C. Wang, D. Lu, W. Ma, S.A. Kube, J. Ma, M. Elimelech, Janus electrocatalytic flow-through membrane enables highly selective singlet oxygen production, Nat. Commun. 11 (1) (2020) 6228, https://doi.org/10.1038/ s41467-020-20071-w
- [64] C. Yu, Z. Zhao, Y. Zong, L. Xu, B. Zhang, D. Wu, Electric field-enhanced coupled with metal-free peroxymonosulfate activactor: the selective oxidation of nonradical species-dominated system, Water Res. 227 (2022) 119323, https://doi. org/10.1016/j.watres.2022.119323.
- [65] M.P. Rayaroth, U.K. Aravind, G. Boczkaj, C.T. Aravindakumar, Singlet oxygen in the removal of organic pollutants: an updated review on the degradation pathways based on mass spectrometry and DFT calculations, Chemosphere 345 (2023) 140203, https://doi.org/10.1016/j.chemosphere.2023.140203.
- [66] Y. Yan, Z. Wei, X. Duan, M. Long, R. Spinney, D.D. Dionysiou, R. Xiao, P.J. J. Alvarez, Merits and limitations of radical vs. nonradical pathways in persulfate-based advanced oxidation processes, Environ. Sci. Technol. 57 (33) (2023) 12153–12179, https://doi.org/10.1021/acs.est.3c05153.
- [67] A.A. Ghogare, A. Greer, Using singlet oxygen to synthesize natural products and drugs, Chem. Rev. 116 (17) (2016) 9994–10034, https://doi.org/10.1021/acs. chemrev.5b00726.
- [68] R.E. Connick, The interaction of hydrogen peroxide and hypochlorous acid in acidic solutions containing chloride ion, J. Am. Chem. Soc. 69 (6) (1947) 1509–1514, https://doi.org/10.1021/ja01198a074.
- [69] C.S. Foote, S. Wexler, W. Ando, R. Higgins, Chemistry of singlet oxygen. IV. Oxygenations with hypochlorite-hydrogen peroxide, J. Am. Chem. Soc. 90 (4) (1968) 975–981, https://doi.org/10.1021/ja01006a023.
- [70] P.M. Wood, The redox potential of the system oxygen—superoxide, FEBS Lett. 44 (1) (1974) 22–24, https://doi.org/10.1016/0014-5793(74)80297-8.
- [71] Y.A. Ilan, D. Meisel, G. Czapski, The redox potential of the O₂-O-2 system in aqueous media, Isr. J. Chem. 12 (4) (1974) 891–895, https://doi.org/10.1002/iicb.197400079
- [72] K.M. Sutherland, S.D. Wankel, C.M. Hansel, Dark biological superoxide production as a significant flux and sink of marine dissolved oxygen, Proc. Natl. Acad. Sci. 117 (7) (2020) 3433–3439, https://doi.org/10.1073/pnas.1912313117.
- [73] M. Hayyan, M.A. Hashim, I.M. AlNashef, Superoxide ion: generation and chemical implications, Chem. Rev. 116 (5) (2016) 3029–3085, https://doi.org/10.1021/acs. chemosys 5100407
- [74] X. Li, Improved pyrogallol autoxidation method: a reliable and cheap superoxidescavenging assay suitable for all antioxidants, J. Agric. Food Chem. 60 (25) (2012) 6418–6424, https://doi.org/10.1021/jf204970r.
- [75] S. Yang, P. Wu, J. Liu, M. Chen, Z. Ahmed, N. Zhu, Efficient removal of bisphenol A by superoxide radical and singlet oxygen generated from peroxymonosulfate activated with Fe⁰-montmorillonite, Chem. Eng. J. 350 (2018) 484–495, https://doi.org/10.1016/j.cei.2018.04.175.
- [76] D.T. Sawyer, J.S. Valentine, How super is superoxide? Acc. Chem. Res. 14 (12) (1981) 393–400, https://doi.org/10.1021/ar00072a005.
- [77] X. Cheng, H. Guo, Y. Zhang, X. Wu, Y. Liu, Non-photochemical production of singlet oxygen via activation of persulfate by carbon nanotubes, Water Res. 113 (2017) 80–88, https://doi.org/10.1016/j.watres.2017.02.016.
- [78] S. Zhu, X. Li, J. Kang, X. Duan, S. Wang, Persulfate activation on crystallographic manganese oxides: mechanism of singlet oxygen evolution for nonradical selective degradation of aqueous contaminants, Environ. Sci. Tech. 53 (1) (2019) 307–315, https://doi.org/10.1021/acs.est.8b04669.
- [79] X.-J. Chen, C.-W. Bai, Y.-J. Sun, X.-T. Huang, B.-B. Zhang, Y.-S. Zhang, Q. Yang, J.-H. Wu, F. Chen, pH-driven efficacy of the ferrate(VI)–peracetic acid system in swift sulfonamide antibiotic degradation: a deep dive into active species evolution and mechanistic insights, Environ. Sci. Tech. 57 (48) (2023) 20206–20218, https://doi.org/10.1021/acs.est.3c06370.
- [80] L. Zhang, Y. Fu, Z. Wang, G. Zhou, R. Zhou, Y. Liu, Removal of diclofenac in water using peracetic acid activated by zero valent copper, Sep. Purif. Technol. 276 (2021) 119319, https://doi.org/10.1016/j.seppur.2021.119319.
- [81] H. Wang, S. Wang, Y. Liu, Y. Fu, P. Wu, G. Zhou, Degradation of diclofenac by Fe (II)-activated bisulfite: kinetics, mechanism and transformation products, Chemosphere 237 (2019) 124518, https://doi.org/10.1016/j. chemosphere.2019.124518.
- [82] R. Qu, B. Xu, L. Meng, L. Wang, Z. Wang, Ozonation of indigo enhanced by carboxylated carbon nanotubes: performance optimization, degradation products,

- reaction mechanism and toxicity evaluation, Water Res. 68 (2015) 316–327, https://doi.org/10.1016/j.watres.2014.10.017.
- [83] J. Ou, J. Deng, Z. Wang, Y. Fu, Y. Liu, Heat induced superfast diclofenac removal in Cu(II)–activated peracetic acid system: mediation from non-radical to radical pathway, Chemosphere 338 (2023) 139528, https://doi.org/10.1016/j. chemosphere.2023.139528.
- [84] J. Zhao, Y. Liu, Q. Wang, Y. Fu, X. Lu, X. Bai, The self-catalysis of ferrate (VI) by its reactive byproducts or reductive substances for the degradation of diclofenac: kinetics, mechanism and transformation products, Sep. Purif. Technol. 192 (2018) 412–418, https://doi.org/10.1016/j.seppur.2017.10.030.
- [85] J. Deng, H. Wang, Y. Fu, Y. Liu, Phosphate-induced activation of peracetic acid for diclofenac degradation: kinetics, influence factors and mechanism, Chemosphere 287 (2022) 132396, https://doi.org/10.1016/j.chemosphere.2021.132396.
- [86] S. Chong, G. Zhang, N. Zhang, Y. Liu, T. Huang, H. Chang, Diclofenac degradation in water by FeCeO_x catalyzed H₂O₂: influencing factors, mechanism and pathways, J. Hazard. Mater. 334 (2017) 150–159, https://doi.org/10.1016/j. ibazznat 2017 04 008
- [87] H. Xu, Y. Sheng, New insights into the degradation of chloramphenicol and fluoroquinolone antibiotics by peroxymonosulfate activated with FeS: performance and mechanism, Chem. Eng. J. 414 (2021) 128823, https://doi.org/10.1016/j. cai/2021.128823
- [88] J. Lin, J. Zou, H. Cai, Y. Huang, J. Li, J. Xiao, B. Yuan, J. Ma, Hydroxylamine enhanced Fe(II)-activated peracetic acid process for diclofenac degradation: efficiency, mechanism and effects of various parameters, Water Res. 207 (2021) 117796, https://doi.org/10.1016/j.watres.2021.117796.
- [89] J. Li, Y. Wan, Y. Li, G. Yao, B. Lai, Surface Fe(III)/Fe(II) cycle promoted the degradation of atrazine by peroxymonosulfate activation in the presence of hydroxylamine, Appl. Catal. B 256 (2019) 117782, https://doi.org/10.1016/j. apcatb.2019.117782.

- [90] J. Wang, S. Wang, Reactive species in advanced oxidation processes: formation, identification and reaction mechanism, Chem. Eng. J. 401 (2020) 126158, https://doi.org/10.1016/j.cej.2020.126158.
- [91] J.-M. Lin, H. Arakawa, M. Yamada, Flow injection chemiluminescent determination of trace amounts of hydrogen peroxide in snow-water using KIO₄–K₂CO₃ system, Anal. Chim. Acta 371 (2) (1998) 171–176, https://doi.org/ 10.1016/S0003-2670(98)00304-3.
- [92] N. Liu, F. Ding, C.-H. Weng, C.-C. Hwang, Y.-T. Lin, Effective degradation of primary color direct azo dyes using Fe⁰ aggregates-activated persulfate process, J. Environ. Manage. 206 (2018) 565–576, https://doi.org/10.1016/j. iesurgap. 2017.11.006
- [93] P. Sun, H. Liu, M. Feng, Z. Zhai, Y. Fang, X. Zhang, V.K. Sharma, Strategic combination of N-doped graphene and g-C3N4: Efficient catalytic peroxymonosulfate-based oxidation of organic pollutants by non-radicaldominated processes, Appl. Catal. B 272 (2020) 119005, https://doi.org/10.1016/ i.apcatb.2020.119005.
- [94] Z. Cao, H. Li, G.V. Lowry, X. Shi, X. Pan, X. Xu, G. Henkelman, J. Xu, Unveiling the role of sulfur in rapid defluorination of florfenicol by sulfidized nanoscale zerovalent iron in water under ambient conditions, Environ. Sci. Tech. 55 (4) (2021) 2628–2638, https://doi.org/10.1021/acs.est.0c07319.
- [95] J. Zhang, D. Wang, F. Zhao, J. Feng, H. Feng, J. Luo, W. Tang, Ferrate modified carbon felt as excellent heterogeneous electro-Fenton cathode for chloramphenicol degradation, Water Res. 227 (2022) 119324, https://doi.org/10.1016/j. watres.2022.119324.
- [96] R. Yin, W. Guo, N. Ren, L. Zeng, M. Zhu, New insight into the substituents affecting the peroxydisulfate nonradical oxidation of sulfonamides in water, Water Res. 171 (2020) 115374, https://doi.org/10.1016/j.watres.2019.115374.
- [97] Y. Li, H. Dong, L. Li, J. Xiao, S. Xiao, Z. Jin, Efficient degradation of sulfamethazine via activation of percarbonate by chalcopyrite, Water Res. 202 (2021) 117451, https://doi.org/10.1016/j.watres.2021.117451.